Unraveling the potential of a biological hammer through biorobotics

Application on *Doedicurus*

Olivier Lonneux
Student number: 275127

Master Thesis Report

Supervision:	Prof. Auke Jan Jjspeert Prof. Ardian Jusufi Prof. Torsten M. Scheyer Dr. Kevin Le Verger
Started:	20 February 2023
Submitted:	23 June 2023
Faculty:	School of Engineering, EPFL

Acknowledgements

I would like to express my gratitude to Prof. Auke Ijspeert, Prof. Ardian Jusufi, Prof. Torsten M. Scheyer, and Dr. Kevin Le Verger for the opportunity to undertake this thesis and their guidance throughout the project. I am thankful to François Longchamp for dedicating time and effort in assisting me with the development of the robotic model. I extend my appreciation to Angelo Scioscia, Alex Stutz, and Bernhard Weisse from the Swiss Federal Laboratories for Materials Science and Technology for their valuable contributions to the construction of a potential full-scale model. I am grateful to Dr. Alessandro Crespi and Astha Gupta for their assistance in providing the necessary research materials. Lastly, my thanks go to Gizéh Rangel De Lazaro, Gabriel Aguirre Fernandez, Jorge Domingo Carrillo Briceño, Nicole Ramstein, and Marcelo R. Sanchez-Villagra for their invaluable work at the Paleontological Institute and Museum of Zürich, which played a crucial role in making this project possible.

Abstract

Doedicurus D. clavicaudatus was a colossal Pleistocene mammal which was equipped with a formidable clubbed tail. Such club are generally assumed to have been used for agonistic behaviour. This thesis investigates the impact properties and optimal motion strategy of this weaponized tail. By utilizing simulations and a robotic model, it builds upon previous studies and emphasizes the significance of body movement in enhancing the tail club's impact. The observed range of club velocity aligns with existing research, suggesting its potential to fracture the carapace of other glyptodonts in intra-specific combat. This work further demonstrates how robotics tools can be valuable for paleontological and biological research.

Contents

1. Introduction

Glyptodonts (Mammalia: Xenarthra) represent the epitome of mammalian defensive capabilities. These colossal armadillos of the Pleistocene era could weight up to 2 tons and were equipped with a heavy bony armour covering almost their entire body. Undoubtedly, these South American mammals posed a formidable challenge to any predator. Nevertheless, they all became extinct during the early Holocene [8].

Some glyptodonts had the particularity of having a bony sheath at the distal end of their tail, which could have been used to strike a predator or to fight in interspecific combat. This type of defence is not exclusive to glyptodont, a similar clubbed tail can be found on ankylosaurs, a group of dinosaur. In facts, despite being from distant families, ankylosaurs and glyptodont are supposed to have undergone a similar evolution of tail traits to acquire such weaponry [4].

The club of *Doedicurus D. clavicaudatus* (Figure 1.1) is the largest which was ever found on any glyptodont member. Doedicurus was approximately 4 meter long and was estimated to weight approximately 1'400 kg [13]. The club alone could have been up to 65 kg heavy and more than 1 meter long [5]. It was likely equipped with spikes, as suggested by the large fossae at the tip of the club (see Figure 1.2).

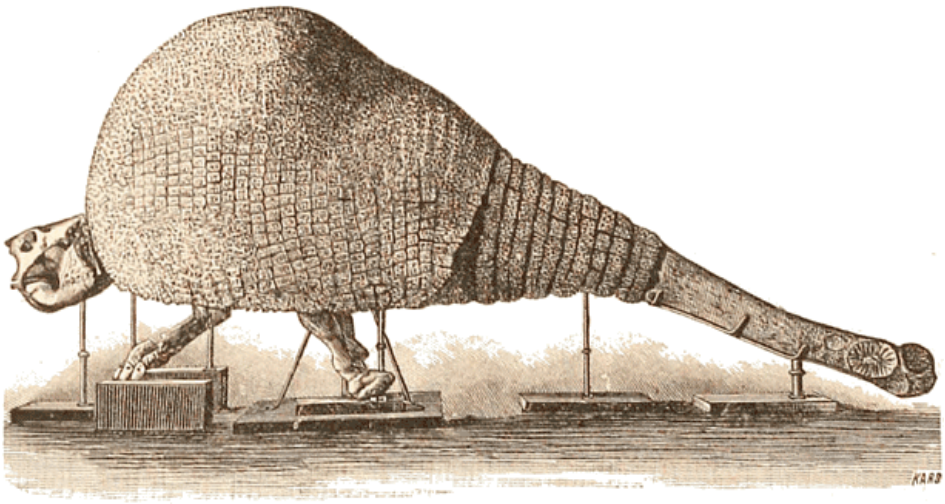

Figure 1.1: Reproduction of *Doedicurus D. clavicaudatus*, James D. Dana, 1894, [7]

The purpose of this club, whether for intraspecific combat, or defence against predators. as well as its effectiveness in damaging the intended target, remain intriguing questions of research.

Some studies have addressed those questions. In 1999, R.M. Alexander and colleagues estimated the energy *Doedicurus* could transmit with a swing of its tail and concluded that the force of impact could be sufficient to fracture the carapace of a congener [2]. In 2009, R.E Bianco and colleagues estimated the position of the centre of percussion of glyptodont's tail club [5]. Their results matched the position of the hypothetical spikes on the tip of the tail, supporting the idea of agonistic behaviour. The general assumption is that such tail was probably not very efficient against fast moving predator and was used mainly for in-

Figure 1.2: Dorsal and lateral view of the Doedicurus clavicaudatus caudal tube (PIMUZ A/V 459) Scale bar = 10 cm. Modified from K. Le Verger (2023) [22].

traspecific combats, as suggested by fractures found on several glyptodont' carapaces [14].

The Palaeontological Institute and Museum of the University of Zurich is currently housing xenarthrans fossils from the collection of Santiago (Kaspar Jakob) Roth (1850–1924) [22]. Among the specimens, there is an almost complete fossilized Doedicurus caudal tube (PIMUZ A/V 459), which gave the opportunity to contribute to the research on the usage of such clubs.

Estimating the force of impact of such a tail is not a simple task, considering the amount of missing data. Alexander and colleagues study [2] used simple assumptions based on the volume of muscles and assumed an almost perfect transmission of kinetic energy into the blow. In 2005, K. Carpenter and colleagues used a more complex method to estimate the impact force of *Stegosaurus* [6], modelling the tail as a series of rigid link and using the cross-section of muscles around each of them, to find the torques and therefore the acceleration of each link. This method was slightly updated and reused by V.M. Arbour in 2009 to estimate the impact force of an *Ankylosaurus* tail club [3].

In the context of studying weaponized tails, the integration of robotic approaches can be particularly valuable. Animal-inspired robots are increasingly being used for biological and engineering research. Biorobots can be used to simulate and analyse the movements of animals [16]. Indeed, robots provide a mean to access and analyse variables that are challenging to measure directly on animals. They have been used to investigate biped [15], quadruped [27], swimming [21], flying [9], climbing [19] and crawling [23] locomotion.

While neuroscience and biomechanics are the primary beneficiary of such studies, robots have also been proven to be useful for evolutionary and palaeontology research. In 2007, to investigate the evolutionary changes from aquatic to terrestrial locomotion, the Biorobotics laboratory at EPFL designed an amphibious robot based on salamanders, which are closely resembling to the first terrestrial animals [17]. This robot was used to test neural circuits that can easily switch between swimming and walking. In 2019, the same laboratory, together with a team at Humboldt-Universität zu Berlin [25] developed a methodology for identifying the most likely gaits of extinct animals. A robot reproduction of *Orobates*, an extinct genus

of diadectid reptiliomorphs, was used to test hundreds of different gaits to determine which one was probably used. Similar concepts can be applied to the analysis of an armoured tail club.

When swinging its tail in a conflictual situation, *Doedicurus* had most likely two objectives. Firstly, to inflict as much damage as possible to the opponent, and secondly to optimize the amount of energy expended during the strike. Based on this assumption, the optimal strategy of motion is also the one which was most likely used. This thesis focuses on investigating the optimal motion strategy associated with these objectives and proposes a method to estimate the impact properties of the weaponized tail. Drawing upon previous studies and complementing them with robotic experimentation, it utilizes simulations and a robotic model of a *Doedicurus* tail.

2. Method and design

2.1. Tail modelling

An accurate representation of the tail had to be modelized to be implemented both in the simulations and for the robotic model. The final 3D model of the tail is shown on Figure 2.1.

Figure 2.1: Model of the tail used in the simulations, the club length is 1 meter

Modelling the caudal sheath

As the fossil of the caudal bony sheath is incomplete, the missing part had to be reconstituted for the club to be implemented in the simulations. The paper from Enersto Bianco and colleagues gives precise measurement of the complete caudal sheath of a *Doedicurus* from the Museo Nacional de Historia Natural in Montevideo (MNHN 2205, Figure 2.2)[5]. The first approach to estimate the length of the club was to compare the minimum and maximum height and width and take the average ratio to get an estimation of the original length of the club. The measurements can be found in Table 2.1.

Parameter	MNHN 2205	PIMUZ A/V 459	Ratio
Max. transverse diameter [mm]	350	302	1.16
Min. transverse diameter [mm]	173	166	1.05
Max. anteroposterior diameter [mm]	217	187	1.16
Min. anteroposterior diameter [mm]	147	132	1.11

Table 2.1: Comparison of measurements between MNHN 2205 and PIMUZ A/V 459

The average ratio is 1.12. As the club MNHN 2205 is 105 cm long, this means the length of the club should be around 94 cm. This looked too short since the maximum length of the incomplete version is already 93 cm, and a good portion of the sheath seems to be missing when comparing its shape with complete cauda tubes. Looking at the photos of

the *Doedicurus* club from the Museo de la Plata (MLP-DP 16-23) (Figure 2.3), the length to width and length to height ratio is larger than the one from the Museo Nacional de Historia Natural, suggesting that those ratios are not constant between individuals. It was finally subjectively decided to assume a complete length of 100 cm, a coherent value considering the shape of our model. The model was completed in Fusion 360, so it would be close to the shape of completes caudal sheaths. The result is depicted on Figure 2.4.

The club of *Doedicurus* originated from fused ring scutes. This means only the outside of the club is made of bones, while the inside was likely composed of tissues and bones. E. Blanco and colleagues [5] assumed a $2000\,\mathrm{kg/m^3}$ for the external density and $1400\,\mathrm{kg/m^3}$ for the internal density. Which resulted in an average density of approximately $1800\,\mathrm{kg/m^3}$. To simplify, the same average density was used, and the club was considered homogeneous. The volume of the reconstituted version of the club used to calculate the mass is the one from the reconstituted version, resulting in a weight of 43.6 kg.

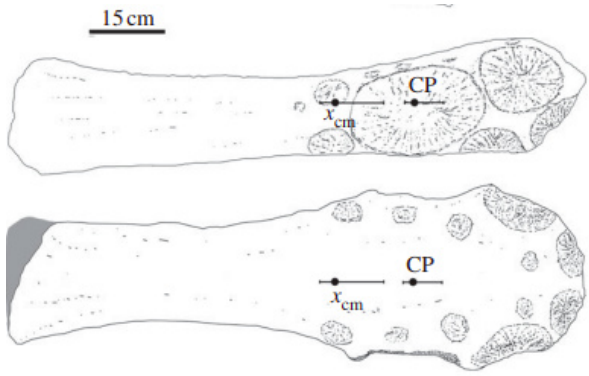

Figure 2.2: Lateral and dorsal view of a Doedicurus caudal sheath (Museo Nacional de Historia Natural, MNHN 2205), with the positions of the centre of mass and centre of percussion, from E. Blanco (2009)[5]

Figure 2.3: Lateral view of a complete armour of Doedicurus (Museo de La Plata, MLP-DP 16-23), from Richard A. Fariña (2002) [12]

Figure 2.4: Comparison of the original model of the club (textured) and its reproduction (white), in lateral (left) and dorsal view (right). Scale bar is 50 cm. The caudal bony sheath was scanned at the Palaeontological Institute and Museum of the University of Zurich by Gizéh Rangel De Lazaro with an Artec Surface scanner

Modelling the proximal part of the tail

The proximal part of the tail is composed of 6 caudal rings. As specimens of *Doedicurus* are incomplete, it was assumed that its anatomy was close to the one of its relative, *Panochtus* (see Figure 2.5). *Panochtus* was a little bit smaller than *Doedicurus*, but had a similar club and the same number of caudal ring. Each caudal ring was attached to one mobile caudal

vertebra, and the remaining space composed mainly of muscles [2]. Based on this information, this part of the tail was modelled as 6 rigid cylindrical links with a hinge joints between each of them.

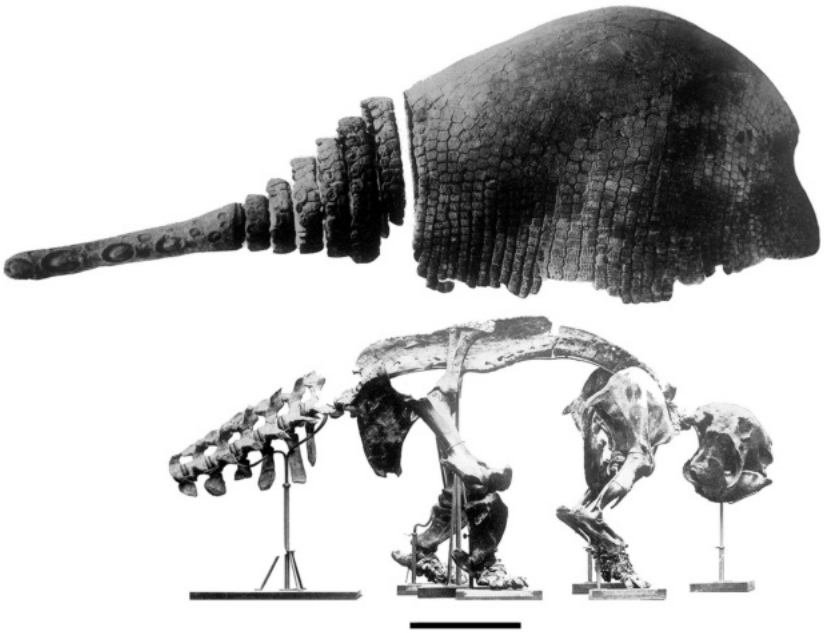

Figure 2.5: Lateral view of the carapace and the skeleton of *Panochtus* (MLP 16-29), mounted under the direction of F. Ameghino. Reproduced and slightly modified from Lydekker (1895, plates 22, 23). Scale bar = 50 cm. [30]

To find the mass of the proximal part of the tail, the cross-sectional radius of each link is needed. Based on observations of MLP-DP-16-23 (Figure 2.3), each ring is approximately 20% larger than the next one. Since each ring scutes is around 11 cm long, the radius of each ring can be found from equation 2.1 with $V_{tot} = 0.105$ and $w = 0.11$.

$$V_{tot} = \pi w(r_1^2 + r_2^2 + ... + r_6^2) = \pi w((1 + (1.2)^2 + ... + (1.2^5)^2))r_6^2 \tag{2.1}$$

The volume of each cylinder can be determined by calculating its cross-sectional area based on the radius, and multiplying by its height (100 cm). Then, assuming the volume unoccupied by muscles were occupied by bones and scutes, the weights of each segment can be calculated using $1060\,\mathrm{kg/m^3}$ for muscle density and a density of $2000\,\mathrm{kg/m^3}$ for bones and scutes [2] [5]. All masses are detailed in Table 2.2.

Segment	Radius [cm]	Width [cm]	Volume [m^3]	Muscle volume [m^3]	Bone volume [m^3]	Muscle mass [kg]	Bone mass [kg]	Total mass [kg]
1	32.34	11	36136	24091	12045	25.54	24.09	49.63
2	26.95	11	25095	16730	8365	17.73	16.73	34.46
3	22.46	11	17427	11618	5809	12.31	11.62	23.93
4	18.71	11	12102	8068	4034	8.55	8.07	16.62
5	15.60	11	8404	5603	2801	5.94	5.60	11.54
6	13.00	11	5836	3891	1945	4.12	3.89	8.02
Club	-	-	22180	5078	19102	5.38	38.20	43.59

Table 2.2: Mass of each link, the total mass of the tail is 188 kg.

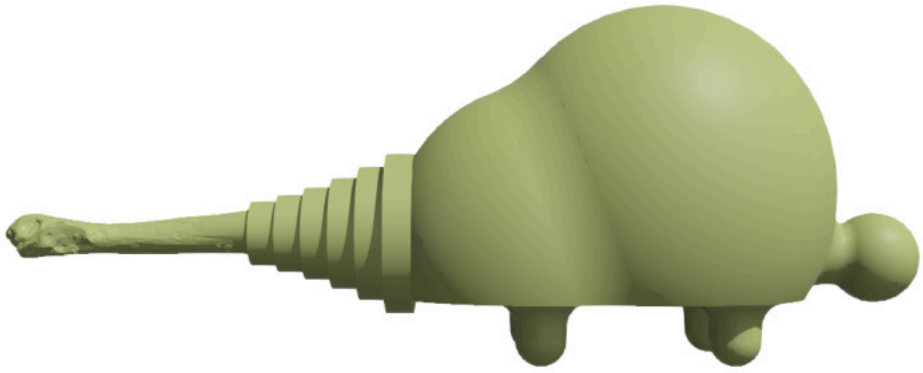

Figure 2.6: Lateral view of the complete model used in the simulations, the caudal sheath is 1 meter long

Modelling the body

The model of the body was created to reproduce the dimensions of *Doedicurus*. It is composed of a single, homogeneous mass. The weight of the body was set to 1250 kg so that the total weight would be close to the estimated mass of *Doedicurus*. The full model is shown on Figure 2.6.

Forces and torques

An estimation of the volume of muscles which was used to power the tail can be found in R.M. Alexander and colleagues study [2]. Their muscle geometric model, shown on Figure 2.7, is composed of a truncated cone, representing the muscles in the tail, and a parallelepiped, representing an extension of the epaxial tail muscles dorsal to the sacrum. The volume of the tail cone was found to be $0.105\,\mathrm{m}^3$, with $0.019\,\mathrm{m}^3$ occupied by ring scutes and $0.017\,\mathrm{m}^3$ being occupied by vertebrae, this leave around $0.07\,\mathrm{m}^3$ being occupied by muscles. The volume of the parallelepiped extension was estimated to be $0.032\,\mathrm{m}^3$. Those estimations were used for all calculations.

To find the forces and torque which can be applied by the muscles to power the tail, the same method as V.M. Arbour paper on Ankylosaurs was used[3]. The cross-sectional area of muscles of each segment can be computed from the cross-sectional area of the same segment by assuming that the muscles to volume ratio is constant throughout the truncated cone. Since the volume of muscle in the tail is $0.07\,\mathrm{m}^3$, and the tail volume is $0.105\,\mathrm{m}^3$, the area is given by equation 2.2.

$$A_{muscles,x} = \frac{0.07}{0.105}\pi r_x^2 \tag{2.2}$$

The maximum force at the end of each link can be found by multiplying half of the muscle's cross-section area with the specific tension for concentric contraction (Eq. 2.3). This variable is constant throughout vertebrates and is estimated to be approximately $20\,\mathrm{N/cm}^2$ [3]. The cross-sectional area of muscles is divided by 2 since only half of the muscles is used to swing the tail on one side. Afterward, the torque being applied to the next link can be calculated by multiplying the force value with half of the muscle's width (Eq. 2.4).

$$F_x = 20\frac{A_{muscles,x}}{2} \tag{2.3}$$

$$\tau_x = \frac{w}{2}F_x \tag{2.4}$$

The parallelepiped extension is assumed to have a $0.8\,\mathrm{m}^2$ section and a $0.4\,\mathrm{m}^2$ width, the

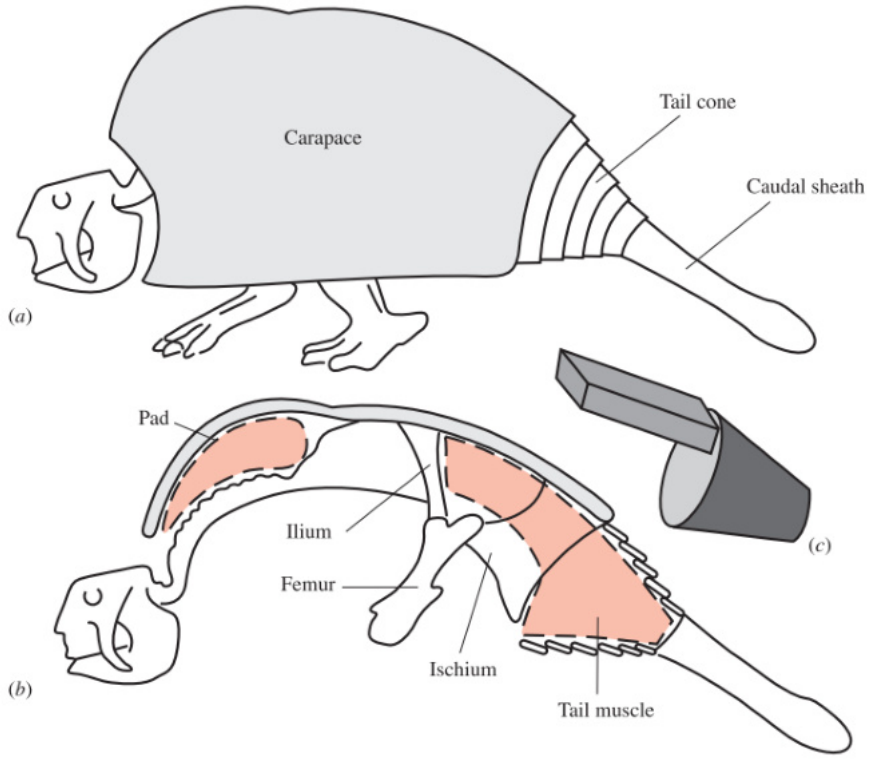

Figure 2.7: Drawings of *Panochthus* (a) A sketch of the intact animal. The 'caudal sheath' is the tail club. (b) Here the armour has been removed from the near side of the body to show the spaces occupied by the tail muscle (c) The geometric model used to estimate the volume of tail muscle." From Alexander R.M. and colleagues [1].

resulting torques and forces are placed at the proximal end of the first link. All torques and intermediates values can be found in Table 2.3.

Segment	Radius of previous segment [cm]	Cross-sectional area [cm^2]	Muscle cross-sectional area [cm^2]	Force [N]	Muscle half width [cm]	Torque [Nm]
1	-	-	810	8100	20	1620
2	32.34	3285	2190	21901	5.5	1205
3	26.95	2281	1521	15209	5.5	836
4	22.46	1584	1056	10562	5.5	581
5	18.71	1100	734	7335	5.5	403
6	15.60	764	509	5093	5.5	280
Club	13.00	531	354	3537	5.5	195

Table 2.3: Torques and forces at the proximal end of each segments

Body rotation

The body may have been used to help power the tail in a synchronized movement. R. Fariña hypothesized that Glyptodonts may have been able to stand on 2 legs and make a step before powering the blow [13], which would have resulted in a 60° body rotation during the movement. The idea that glyptodonts could adopt a bipedal posture comes from the backwards displacement of their centre of mass and from the great proportion of body mass

which was resting on their hind-limbs [29] in comparison with fore-limbs. The idea that glyptodonts could adopt an erect bipedal posture is subject to debates, as the morphology of the carapace and pelvis may not have permitted such a stance[11]. However, they likely could rest their mass completely on the hind limbs while maintaining their body in a horizontal position [11]. Leaving their forelimbs completely free and allowing a greater range of motion when swinging their tail.

On humans, the mean maximum angular velocity of the hip throwing a 6 kg medicine ball is 7.4 rad/s, for a maximum hip angle of around 60 ° [18]. While the movement of a human throwing a medicine ball is significantly different from the body movement that *Doedicurus* would have used to accompany the tail movement, it is possible that their body rotation maximum speed was in the same order of magnitude. Glyptodonts may look like very slow animals with their carapace, but their femora were strong enough for their agility to be comparable to one of a rhinoceros or a buffalo [13]. Therefore, 5 rad/s was considered to be a reasonable estimation of the maximum body angular velocity.

Vertebrae angle of mobility

Figure 2.8: Dorsal view of the caudal vertebrae of *Glyptodon munizi* PIMUZ A/V 463, scale bar is 5 cm (picture from Kevin Le Verger, 2023)

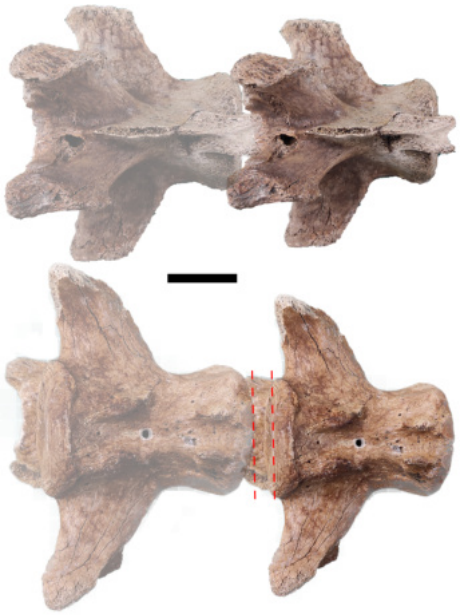

Figure 2.9: Assembly of the vertebrae, in dorsal (top) and ventral (bottom) view, scale bar is 5 cm, the 15 mm intervertebral space is represented by the 2 dotted red lines

Ideally, to find the angle of mobility between each link, a complete skeleton of the tail assembled with respect to the intervertebral discs would be needed. However, such a fossil is not available, meaning an alternative method was used. This method is the same one used by V.M. Arbour [3].

In 2007, Gordon Dzemski and Andreas Christian [10] found that vertebrae flexion was limited by the overlap of the prezygapophyses and postzygpophyses. For camel and ostriches neck, the minimum overlap of the joint facets was between one eighth and one quarter of the maximum value for lateral flexion. The half-angle of mobility they found for those movements was below 25°. Considering the flexibility of camel and ostriches neck, this should be close to an upper bound for vertebrae mobility. Based on those results and by analysing

the overlap of the prezygapophyses and postzygpophyses of two adjacent caudal vertebrae when rotating, the maximum angle of mobility can be estimated.

Caudal vertebrae of a *Glyptodon munizi* fossil from the Palaeontological Institute and Museum of the University of Zurich (PIMUZ A/V 463) were chosen for the measurements. The mobility of the tail of *Glyptodon munizi* was likely similar to the one of *Doedicurus D. clavicaudatus*. as those two species have similar body proportions.

Each vertebra is on average 15% larger than the next one. As the 4th caudal vertebra is the most well-preserved, a dorsal view of the 4th vertebra scaled up by 15% was used to represent the 3rd vertebra. The 2 caudal vertebrae were assembled assuming a 15 mm inter-vertebral disc thickness. This is an arbitrary value, for reference, human intervertebral disc are between 7 and 10 mm thick and a bovine intervertebral disc is around 12 mm thick. The 4th vertebra is rotated in 5° increments, and the overlap area of the postzygapophyse on the prezygapophyse is measured for each one of them. The axis of rotation is located on the half-way point between the two prezygapophyse. All rotations are shown on figure 2.10.

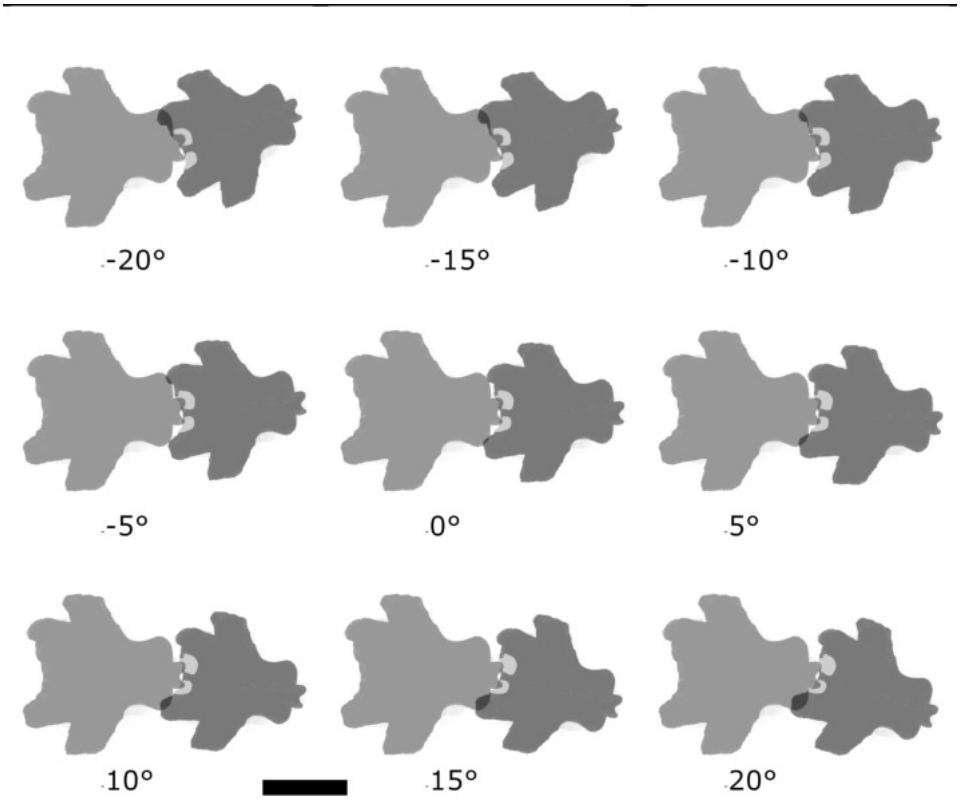

Figure 2.10: Dorsal view of the caudal vertebrae assembly with various angles of mobility, the prezygapophyse are in light grey, the overlap in dark grey, scale bar is 10 cm

Table 2.4 shows the overlap percentage with various angles. Based on those data, the half-angle of mobility was likely around 10°. With a -5 degrees rotation, the right overlap ratio is around a quarter of the overlap ratio at a 15° rotation, and inversely for the left overlap ratio. The middle point is away from zero, which is probably due to some initial misalignment of the vertebrae.

Vertebra Angle [°]	Left overlap area [mm^2]	Right overlap area [mm^2]]	Left overlap ratio [%]	Right overlap ratio [%]
-20	137.19	0.00	38.08	0.00
-15	118.18	3.39	32.80	1.54
-10	97.52	6.94	27.07	3.15
-5	76.03	11.57	21.10	5.25
0	58.60	17.36	16.26	7.87
5	43.80	26.45	12.16	11.99
10	28.93	33.88	8.03	15.36
15	15.70	43.80	4.36	19.86
20	4.96	52.89	1.38	23.98

Table 2.4: Vertebrae overlap data, left and right area of prezygapophyse are $360\,\text{mm}^2$ and $221\,\text{mm}^2$ respectfully

2.2. Simulations design

Two simulations were made which use different supports and different actuation models. The resulting visual rendering of both simulations is depicted on Figure 2.11.

Motor-torque simulation

The first simulation was made on Webots. The tail is powered using only rotational motors. The motors are placed between each segment of the tail, their maximum torques correspond to the ones computed in the previous section. An additional hinge joint powered by a motor was placed at the pelvic location to rotate the body. This motor tries to reach the designed body rotation angle. This motor has a speed cap, which correspond to the maximum body angular velocity. This speed cap is usually reached for a rotation of 60° but not for one of 30°.

Tendon-driven simulation

To try and better emulate the elastic properties of biological tendons and muscles, a Mujoco simulation using tendons and muscle actuators was designed. Mujoco provides a muscle model which is already well tuned for reality. The body, club and tail rings are modelled in the same manner as the previous simulations.

Only two tendons are used as the movement is only simulated horizontally, each one starts at the base of the tail muscle extension and finishes at the base of the club. Both of them go through the half-way point between the centre of the muscles and the exterior of the muscles. The muscles forces were set to the sum of the forces of each joint as calculated previously, which is $71\,636$ N for each side of the tail. The maximum tendon elongation was kept at 5%, a reasonable value for most biological tendon [28].

The body rotation is simulated in the same manner as the motor-driven simulation. The difference is the Mujoco does not support speed limit for its position actuator, to achieve a similar body dynamic to Webots motor control, a torque motor was used and the command is given by a simple PD controller combined with a breaking system. The motor has 2 control mode, one which tried to get close to the target position and ones which reduces the speed of the actuator once it gets too close to the fixed maximum rotation speed. After tuning the parameters, the motor behaviour gets really close to the one in Webots. Mujoco constraints are soft, meaning the solver as to be tuned appropriately for the joints not to transgress their limits. For simplification and a more suitable comparison with Webots,

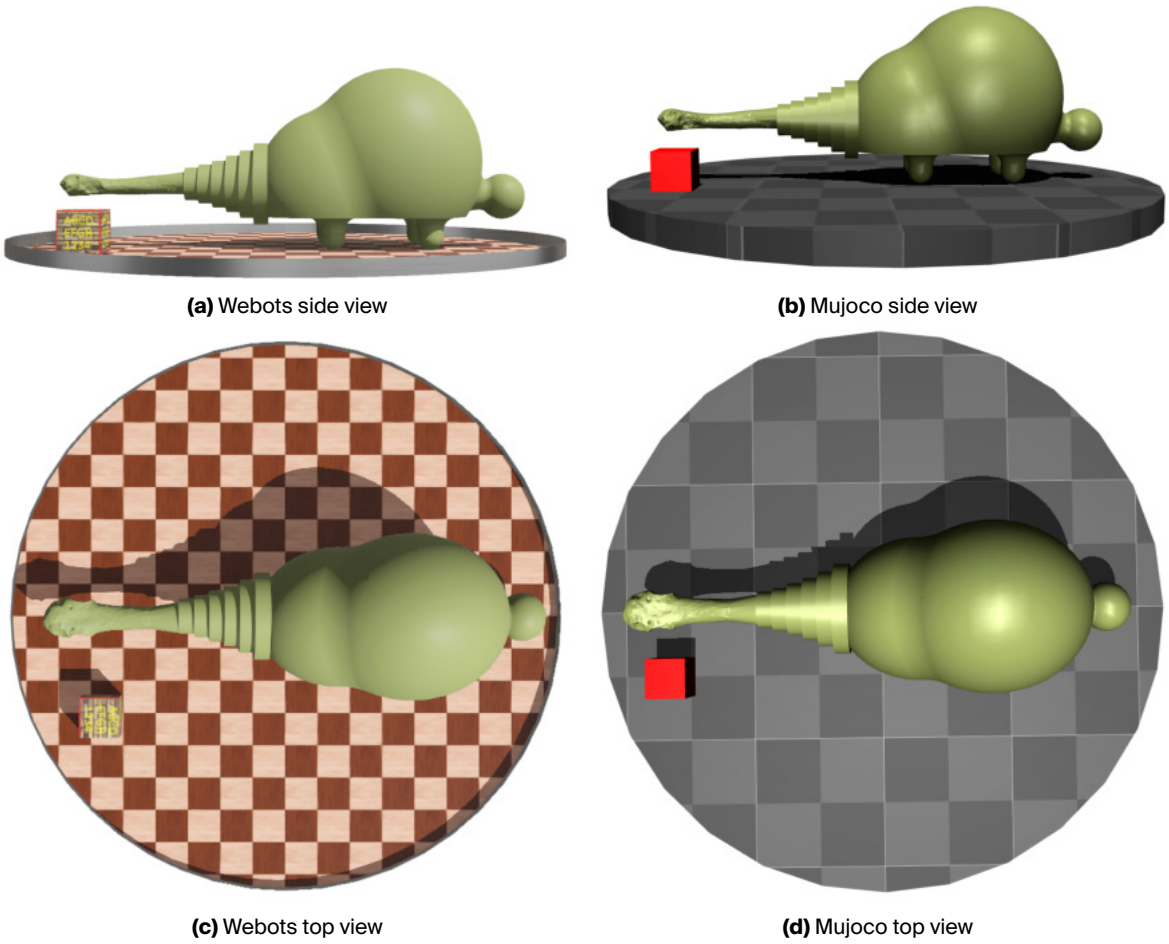

(a) Webots side view

(b) Mujoco side view

(c) Webots top view

(d) Mujoco top view

Figure 2.11: Side and top views of both simulations, boxes are 30 cm wide

this solver was tuned to make the constraints almost completely rigid.

2.3. Robot design

A robotic model of the tail was designed to see how simulations results translate into reality. Just like the simulations, the physical model consists of a copy of the tail with 7 joints and a rotating platform representing the body movement. It is actuated with string attached to a motor, a similar model to the tendon-driven simulation. A rendering of the robot is presented in Figure 2.12.

Size and actuation choice

In an ideal scenario, creating a life-sized model would be the most accurate approach to estimate the speed and impact forces realistically. However, designing and constructing such a robot present significant challenges. The total mass of the model is 188 kg, requiring exceptionally robust joints and powerful actuation mechanisms. Within the project's time frame, developing a robot of this magnitude was difficult.

As a result, two solutions were explored: a full scale model with a simplified dynamic, actuating only the caudal sheath and a small scale model with accurate dynamics. The main idea for the full scale model was to to represent the caudal sheath with a simple round or square rod of around 40 kg, with a mass of bone-like material of approximately 5 kg at the

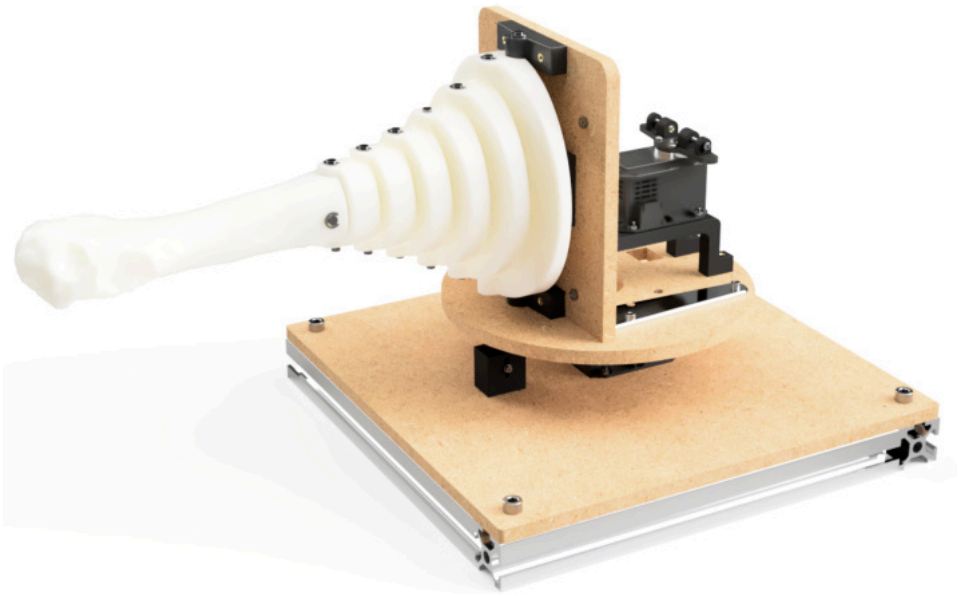

Figure 2.12: Rendering of the robot, the tail club is 17 cm long

extremity. The bony mass would serve both to move the centre of mass of the club to its real location and to simulate bone-like properties at the point of impact. This club would be powered by a 6 kN hydraulic actuator, which, in theory, would be sufficient to reach the speed comparable to the ones in the simulations (assuming all the actuator's energy would be transmitted into the club's kinetic energy). However, the motor would still need to move fast enough, which was not guaranteed considering hydraulic actuators' velocity.

A second idea, was to use a transport chain and covering it with steel tubes to represent the links of the tail. This would result in a model with several joints and could be actuated with steel wire and hydraulic actuator. The mechanical resistance of the chain would have to be carefully assessed to avoid material failure, but this is a simple design solution for a real scale robot. Both project could be realized at the EMPA facility in Zürich but were postponed, as a smaller scale model was prioritized. Illustrations of the materials are shown on Figure 2.13.

(a) Example of rod and bony end to represent the caudal sheath

(b) Transport chain

Figure 2.13: Materials for the potential real scale model

Instead, a miniature model which would represent more accurately the movement of the tail was designed. Two possibilities of actuation were identified: using a motor for each joint or using tendons. A tendon actuation was chosen as it uses only 1 motor instead of 7, which means it is cheaper, lighter and easier to implement. The maximum torques needed

is also less important as the actuation is made with a larger range of movements. It is also more closely related to the actuation of real muscles, as muscles work in contraction and extension and not in rotation.

Two Dynamixel MX-64 motors were already available for use. Those motors have a maximum torque of 6 Nm. To make sure sufficient speed could be reached with those motors, a Mujoco simulation representation of the physical system was designed, and various scale factors were applied. The chosen scale factor is 1/6. A maximum speed of approximately 5 m/s could be reached on a simulation with a maximum motor torque of 6 Nm. With such a scale, the total mass of the tail is divided by 216. Resulting in a weight 870 g and a length of 29 cm.

Tail design

The vertebrae are modelled by a series of cylinder-like shape. The sides of those cylinders are inclined at an angle of 5° to have a half-angle mobility of 10° on each side. The club is modelled as a modified version of the reconstituted model, scaled down by a factor of 6. All those pieces were 3D printed in PA220 using SLS technology by the Additive Manufacturing Workshop of EPFL. Indeed, considering the complexity of the shape of the club, printing it using FDM technology would have been difficult. The pieces dimensions were chosen so that each link would be 216 times lighter than their real counterpart. The axis mass was also taken into account. As PA220 density is $1.1\,\mathrm{g/cm^3}$, way below the estimated density of the club ($1.8\,\mathrm{g/cm^3}$) the club height and width was scaled up by 27% for it to have the appropriate mass while keeping its original length. The details of the calculation can be found in Table 2.5.

Segment	Total Mass Wanted [g]	Diameter [mm]	Axis Mass [g]	Volume [cm^3]	Plastic Mass [g]	Total Mass [g]	Difference [g]
1	230	133	28	187	201,42	230	-0.13
2	159	106	22	127	137,48	160	0.41
3	111	85	18	87	93,56	112	0.78
4	77	68	14	58	62,14	77	-0.38
5	53	55	12	39	41,96	54	0.19
6	37	45	10	26	28,11	38	0.55
Club	202	43	9	174	191,51	201	-0.98

Table 2.5: Links desired and estimated mass in the miniature model, assuming a PA220 density of $1.1\,\mathrm{g/cm^3}$ and an aluminium density of $2.7\,\mathrm{g/cm^3}$

Each cylinder has a 2 mm wide hole on each side for the tendons to go through. Those holes are inclined at a 5 degrees angle, this was done to optimize the range of motion. The larger the distance between the tendons at the motor location, the higher the range of motion. They are connected between each other using 5 mm diameter aluminium axis serving as hinge joint. Circlips were placed on the top end of the axis to keep them in place. There was no need to place one on the bottom, as the tail doesn't to be turned around. Only lateral movements are explored during the experimentations. Locking the axis position on only one side also facilitates the disassembly. To connect the tendons to the caudal sheath, an axis was inserted laterally through its proximal part and two gaps were made on the proximal side of the club to reach it from the outside. This allows the strings to be attached around the axis (see Figure 2.14).

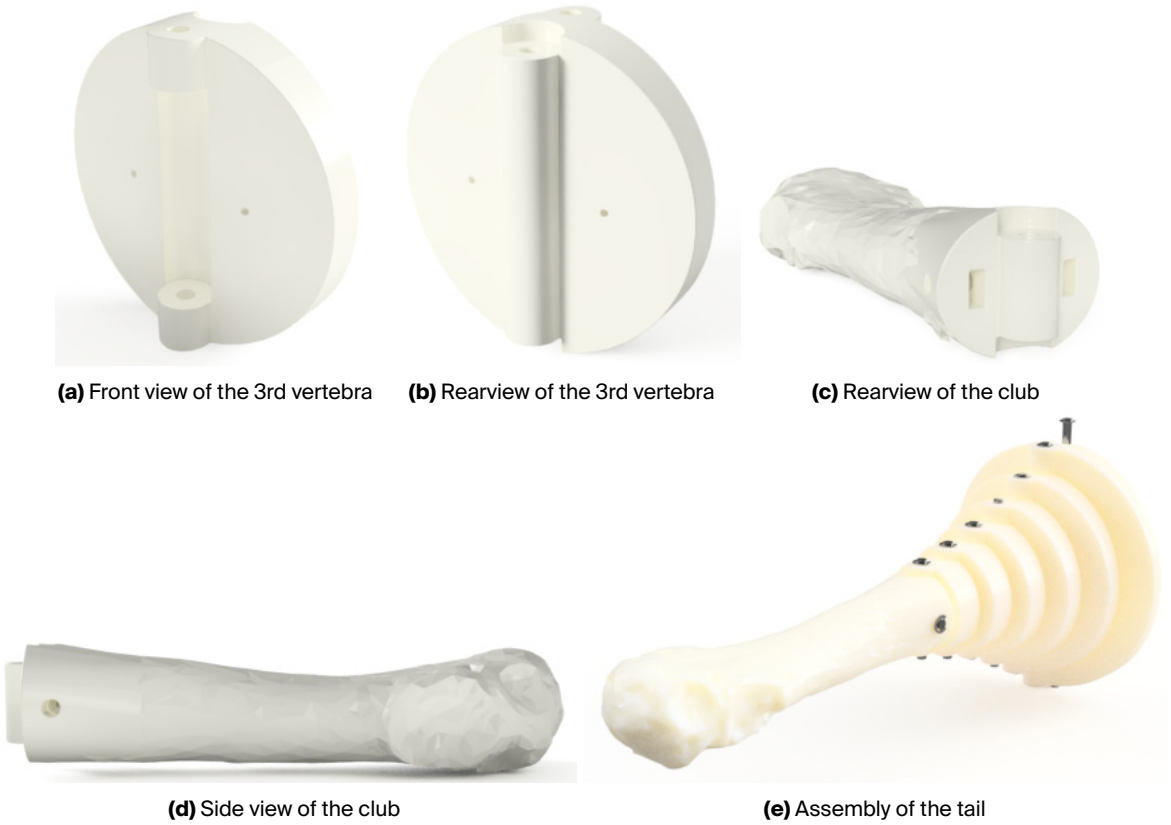

(a) Front view of the 3rd vertebra **(b)** Rearview of the 3rd vertebra **(c)** Rearview of the club

(d) Side view of the club **(e)** Assembly of the tail

Figure 2.14: Renderings of the 3D printed tail

Tendon actuation

The tail is mounted on a MDF plate (Figure 2.15a). To this plate was attached 2 supports for the first axis to go through and 2 stoppers which have the role of stopping the first vertebra at a 10 $^\circ$ angle. All those pieces are fixed on the plate using threaded insert and M3 screws. The plate is mounted on the rotating platform using two 125x150 angle bracket. There are two large holes going through the plates and stopper to let the strings go through.

The MX-64 Dynamixel motor used for tendon actuation is fixed on 2 support pieces which are 3D printed in PLA and fixed to the rotating platform on one side and on the vertical plate on the other side using threaded inserts. A complementary horn was printed in ABS reinforced with carbon and fixed to the motor initial horn. With two 2 mm holes on its extremities to attach the string at the correct distance from the motor shaft. ABS reinforced with carbon is considerably stiffer than PLA, which makes it ideal for this application. This assembly is shown on Figure 2.15b.

On top of the motor horn is a tensioning system. Each side of the system is composed of 2 small pieces. One is fixed on the horn, in which a threaded insert was installed. In this part, a M2.5 screw gets inserted. At the head of the screw, is a simple attachment piece on which the string is attached. The tension of the string can then be controlled by tightening or loosening the screw.

Solid strings are needed to represent the tendons. To avoid frictions loss, the robot was first tested with 0.65 mm wide nylon string. However, due to this low coefficient of friction, the knot became loose after some experimentation. As such, Zeus HPPE Braided Line were

used. Those 0.6 mm wide strings can support a charge of 65 kg and are very rigid, making them ideal once the robot was well calibrated, Tendons were attached on both extremities, before being stretched using the tensioning system.

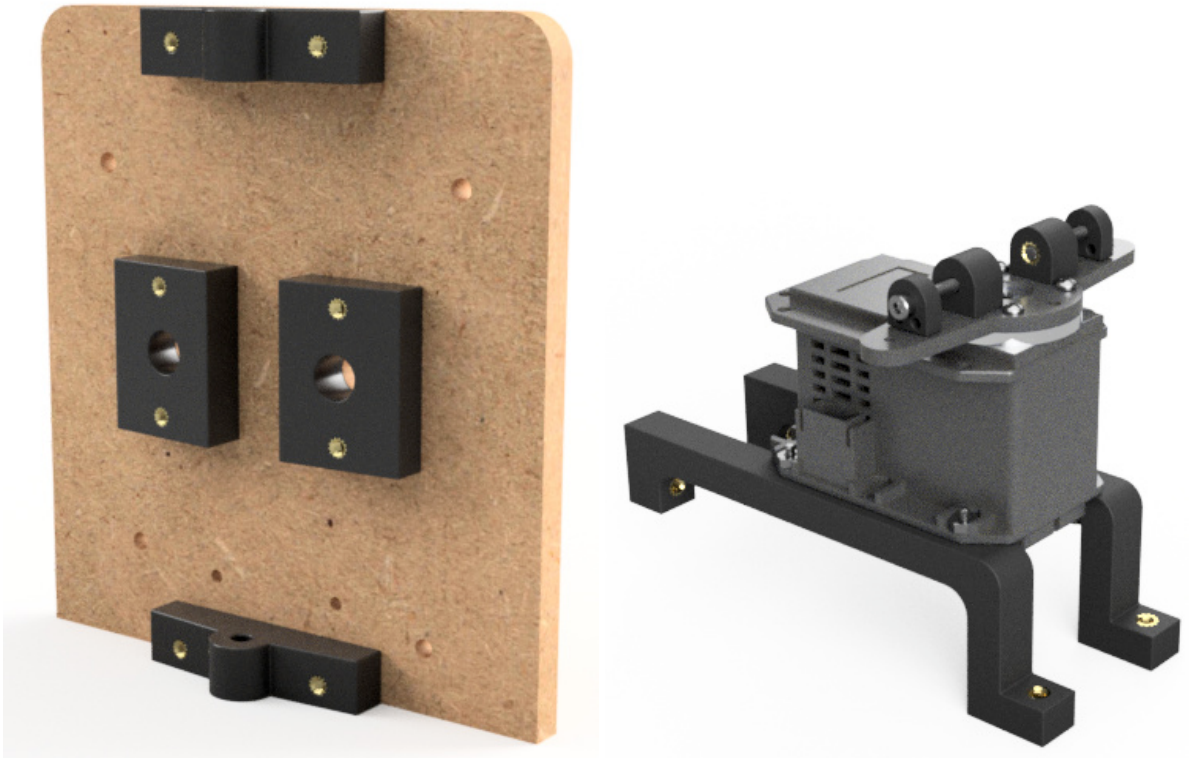

(a) Vertical MDF plate **(b)** Motor assembly

Figure 2.15: Parts on top of the rotating platform

Rotating platform

To simulate the body rotation, the MDF plate is mounted on a rotating MDF platform (Figure 2.16a). This platform is actuated with an MX-64 Dynamixel motor. An aluminium plate was fixed between the motor and the plate to provide additional rigidity. The motor fixed on a square base, which was made using four 25 cm long aluminium profiles and a MDF square plate. While the base is quite heavy on its own, it still needs to be clamped or fixed to avoid any movements during the experimentation.

To provide additional support to the rotating platform and avoid overloading the motor axis, an adjustable support was designed (Figure 2.16b). It is composed of two 3D printed pieces which can be slided into each other. A screw passing through the two pieces can be fastened to lock the system. On the top pieces is a ball bearing mounted on an axis. This bearing comes into contact with the platform and supports it with minimum friction.

Unfortunately, the mass of the rotating platform is too low in comparison with the tail. Since the total mass of the tail is near 1 kg, the mass of the rotating platform should be above 5 kg to keep the tail to body mass ratio of the *Doedicurus*. Additional weight could have been added, but the motor used could not support such a mass and material failure could have happened. Therefore, the system was kept identical.

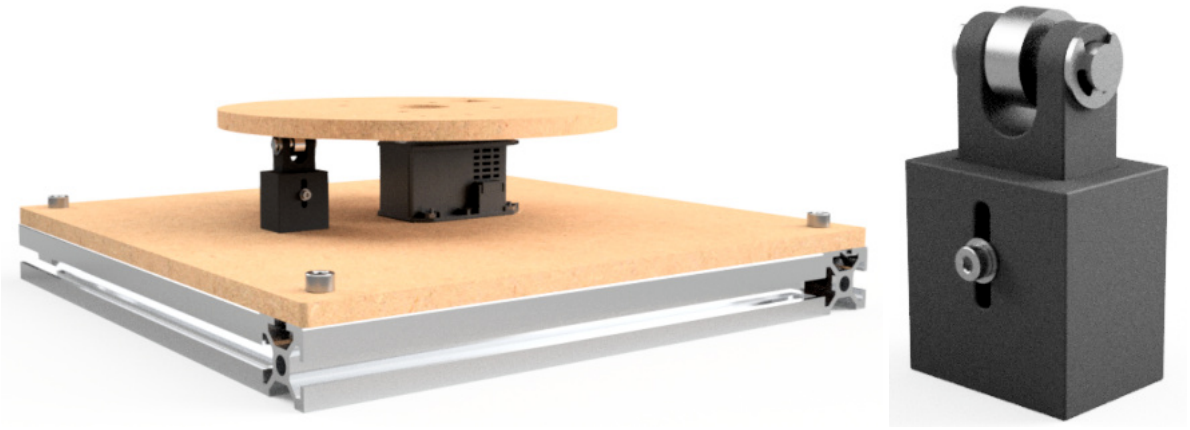

(a) Rotating platform **(b)** Support

Figure 2.16: Rotating platform and support

2.4. Experimentation procedure

Experiments were conducted with the 2 simulations as well as with the physical model. All experiments were performed in the following manner: the tail swings on one side, after a delay, it swings on the other sides and is accompanied by the body rotation. The maximum speed of impact correspond to the maximum speed near the tip of the club, where the spikes were supposed to be.

The following parameters were experimented on:

- **Swing offset [s]** This refers to the delay between the first and second swing of the tail. A swing offset of 0 indicates that there is no initial swing, and the second swing will only perform half of the complete movement. Conversely, a higher swing delay will result in a period of stillness before the second swing occurs. In this study, the initial value of the swing offset was set at 0.4, which is approximately it takes to finish the preliminary swing.
- **Body rotation offset [s]** This is the delay between the start of the body rotation and the start of the second swing. A body rotation offset of 0 results in both movements being performed simultaneously. This parameter is modulated from -0.4 to 0.4 with an initial value set to 0.
- **Body rotation angle [°]** This is the maximum body rotation which is reached during the movement. This parameter is modulated from 0 to 60° with an initial value set to 30°.
- **Body rotation speed [rad/s] or [rev/min]** This is the maximum body rotation speed. It goes from 0 to 10 rad/s with an initial value of 5 for the simulations and from 50 to 300 rev/min with an initial value of 150 for the robot.
- **Half-angle of mobility [°]** This is the maximum half-angle of mobility of each tail joints. It was varied from 5 to 15 with an initial value of 10. Those variations can only be done on the simulations, as the robot was designed to block at a 10° angle.
- **Motor speed [rev/min]** This is the tendon motor velocity of the real model. It was varied from 50 to 500 with an initial value of 300 rev/min
- **Power factor** This is the power factor of the preliminary blow. A factor of 1 means the preliminary swing is made with the same torques, tendons forces, or motor speed as

the damaging blow. A factor of 0.5 means those values would divide by 2. Its initial value is 1, and it was varied from 0 to 1.

- **Tendon-step** This corresponds to the muscle control increase per timestep in the tendon-driven simulation. The maximum control is 1, corresponding to the maximum force being applied to the tendon. It is initially set to one (i.e. maximum control value is instantaneously reached), but different values were tested to limit the contraction speed of the muscles. In other word, this means transforming the control signal from a square signal to a triangular one.

For all experiments, the point of impact was considered to be in the centre of the largest depression at the tip of the tail, where a potential spike may have been located. Recording the speed at this point is straightforward in the simulations using provided sensors. For the real model, a camera was placed on top of the robot to record the movements and a small black marker was put at the tip of the tail. The recording were done with 60 frame per speed and a 1/4000 s shutter speed to avoid motion blurring. The tracking of the position of the club was done using OpenCV template matching algorithm, which provided better results than motion tracking algorithms. A 2 value moving average was applied to the results to avoid the impact of potential outliers. Photos of the robot are represented on Figure 2.17. The experimentation setup is shown on Figure 2.18a, the tracking view can be seen on Figure 2.18b.

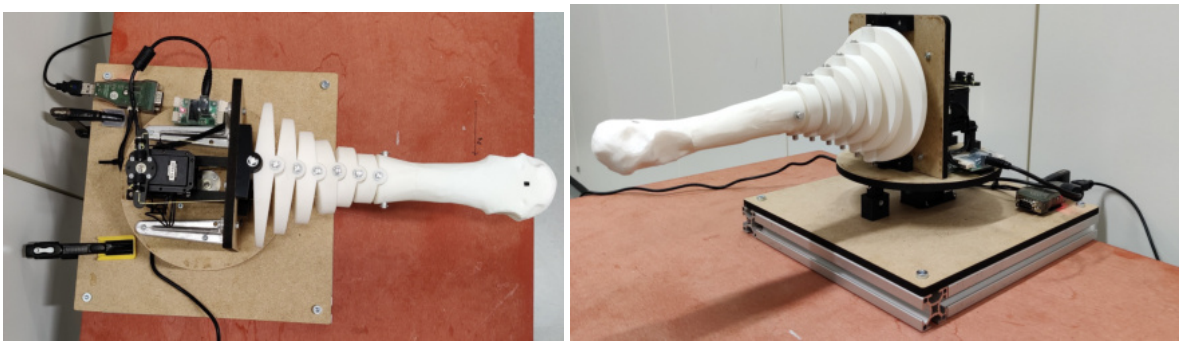

(a) Top view of the robot **(b)** Front view of the robot

Figure 2.17: Photos of the robot

2.5. Metrics

Impulse and force of impact

Monitoring the force of impact when experimenting would require a careful analysis of the material's properties. Testing the impact force on a rigid material would result in an overblown force of impact, and inversely for a material which would be too soft. As a result, the experiments were only used to monitor the speed of the tail. However, the force of impact and other variables can still be derived from the experimentation's data. The impulse of the impact can be computed from the velocity (Eq 2.5).

$$J = m_{club} v_{impact} \tag{2.5}$$

With m_{club} the mass of the club on impact and v_{impact} the speed of the point of impact. With the impulse, the force of impact F can be calculated (Eq. 2.6), as well as the stress σ (Eq. 2.7). With t_{stop} the total duration of the impact and A_{impact} the area of impact.

$$F = \frac{J}{t_{stop}} \tag{2.6}$$

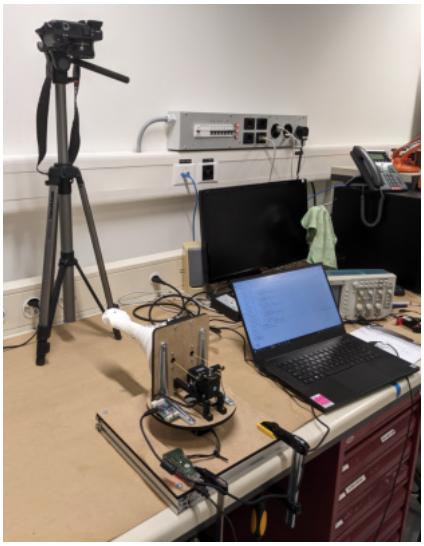

(a) Setup for experiments

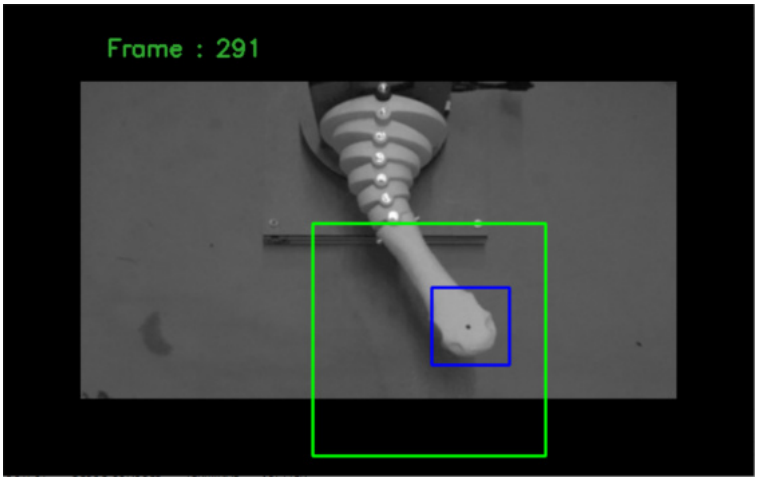

(b) Tracking view during motion, the green and blue square corresponds to the search area and to the tracked area respectively

Figure 2.18: Photos of the experimentation

$$\sigma = \frac{F}{A_{impact}} \tag{2.7}$$

Energy efficiency

To conduct a numerical analysis and estimate the optimal strategy of the animal, evaluating the energy efficiency of the blow (Eq. 2.8) or alternatively, a modified version of the cost of transport (Eq. 2.9) can provide valuable insights into the efficiency and effectiveness of the tail's impact.

$$\eta = \frac{E_{blow}}{E_{used}} \tag{2.8}$$

$$COT = \frac{P_{max}}{mgv_{max}} \tag{2.9}$$

However, using efficiency alone would not adequately capture the impact of the blow on the glyptodont's stamina. Not all muscles are equal in terms of power output. In the case of humans, it is more efficient to generate energy through larger muscles like the legs or the trunk rather than smaller ones like the arms. It is also preferable to share the power output through several muscles than through one. Several metabolic costs, which assess the energy expenditure of metabolisms more accurately, already exists [20]. Unfortunately, they are all fairly complicated and require knowing the value of complex variables such as the heat rates and maximum contractile velocity of the muscles. Instead, a cost of impact was defined (Eq. 2.10).

$$C_{impact,tail/body} = \frac{E_{used,tail/body}}{m_{muscles,tail/body}} \frac{m_{club}}{E_{impact}} \tag{2.10}$$

This cost of impact is dimensionless and takes into account the total mass of muscles available in both the tail and the body to define the impact on the energy usage over the metabolism. Since the maximum energy output of muscles linearly depends on their mass [2], dividing the energy output by the mass of muscles should be a meaningful indicator of the metabolic cost of the movement. The energy of impact was added to have an indication of the "reward" of the strike. Minimizing this value means minimizing the metabolic cost and optimizing the speed of impact.

This indicator does have one flaw: while it is mass independent (the mass of the club simplifies itself in the calculation as $E_{impact} = \frac{1}{2} m_{club} v_{impact}^2$), it is not speed independent. Meaning it cannot be used to compare the robot and the simulations as they both have different output speed. To address this, the speed to club length ratio was used instead of the true velocity when calculating the energy of impact of the robot.

The energy of the blow is considered to be equal to the kinetic energy at the point of impact (Eq.2.11).

$$E_{impact} = \frac{1}{2} m_{club} v_{tip}^2 \tag{2.11}$$

The energy used by the tail and body depends on the experimentation support. For Webots, the energy of the tail is equal to the work of all motors (Eq.2.12).

$$E_{used,webots} = \sum_t \tau_{m,t} \theta_m \tag{2.12}$$

With $\tau_{m,t}$ corresponding to the torque of the motor during timeframe t and $\theta_{motor,t}$ the angle of displacement of the motor during the same timeframe. This can be easily applied to compute the energy of the tail however, since the body is not fixed on a physical support, the simulation cannot calculate the torque feedback of the body motor. Instead, the energy of the body rotation was used (Eq.2.13).

$$E_{used,body} = \sum_t \Delta E_t = \sum_t \frac{1}{2} I(\omega_t^2 - \omega_{t-1}^2), \text{ if } \omega_t > \omega_{t-1} \tag{2.13}$$

With ω_t the angular speed at timeframe t and I the moment of inertia of the body, which is $320\,\mathrm{kg/m^2}$ (computed by the software). The same computation is made for the energy of the body in Mujoco. The tendons' energy is defined by equation 2.14. With $F_{tendon,t}$ corresponding to the norm of the force in the tendon at timeframe t and $d_{tendon,t}$ the displacement of the tendon during the same timeframe.

$$E_{tendon} = \sum_t F_{tendon,t} d_{tendon,t} \tag{2.14}$$

For the real robot, the energy of the system is considered to be the energy used by the motors (Eq. 2.15), with $V = 12V$ corresponding to the tension of the motor, $I_{m,t}$ corresponding to the current flowing through the motor m at timeframe t and Δt the duration of the timeframe.

$$E_{motor,robot} = \sum_t \frac{I_{m,t} V}{\Delta t} \tag{2.15}$$

The mass of muscles in the tail is $108\,\mathrm{kg}$, the mass of muscles in the body is assumed to be 40% of the body mass. This is most likely an overestimation, but it counterbalances the simplification of the body rotation. In the simulations, the whole body mass is rotated around a single axis of rotation. In reality, some of the rotation would be made using the pelvis, meaning only the trunk would need to be rotated and not the legs itself. Therefore, the energy cost associated with tail movement in the simulations is probably higher than what would be observed in the actual organism.

3. Results

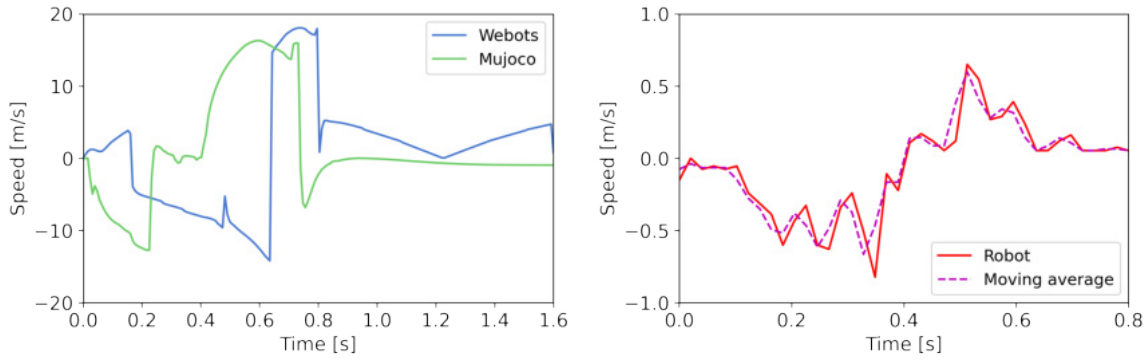

(a) Simulations

(b) Robot and its 2 values moving average

Figure 3.1: Velocity profile with baseline parameters, the value corresponds to the norm, while the sign depends on the direction of the swing

Figure 3.1 shows the different velocity profile with baseline parameters. The velocity sign depends on the direction of the tail movement. The tendon-driven simulations and the robot gets to their maximum speed value faster than the motor-torques one. Figure 3.2 to 3.9 illustrates the influence of the different parameters over the maximum speed of movement.

As anticipated, the robot's swing maximum velocity is considerably lower than the ones from the simulations. This is expected due to the reduced scale of the model. To achieve a similar swing duration, the velocity should be 6 times smaller in robotic testing compared to simulations. However, the observed average slowdown is around 18 times slower, indicating that the tendon motor speed may have been set too low. However, the swing's duration of the robot is actually shorter than the one in the simulations (see Figure 3.1). Which means that the average speed-to-body-length of the robot's club may actually match the ones from the simulations. The lower maximum speed can therefore be attributed to 2 factors. Firstly, the framerate of the camera may have been insufficient to track the true maximum velocity of the tip, and secondly the acceleration of the robot may be noticeably faster than the simulations which would compensate the lower maximum speed.

The swing offset parameter (Figure 3.2) demonstrated a noticeable impact on the simulations, but had a relatively insignificant effect on the robot. In both simulations, the maximum speed increases with the swing offset until reaching a maximum value (from -53% in Webots and from -18% in Mujoco), after which it slightly decreases in the motor simulation (-3%) but stays stable in the tendon-driven one. Suggesting that some of the energy of the preliminary swing may transmit to the second swing in the first simulation but not in the second. Meanwhile, the robot speed is stable throughout those variations, except with very low swing offset, where the maximum speed is marginally higher. There is no reason for this increase in velocity, as the swing distance is shorter in this experiment. The reason behind this improved velocity likely lie in the tensioning of the string. Through experimentations, the string lost some of their tensions. This resulted in a less responsive movement and a reduced maximum speed. Since the string tension was not controlled after every ex-

periment, the first few experiments sometimes showed increased velocity. A similar effect appears with the power factor experimentation.

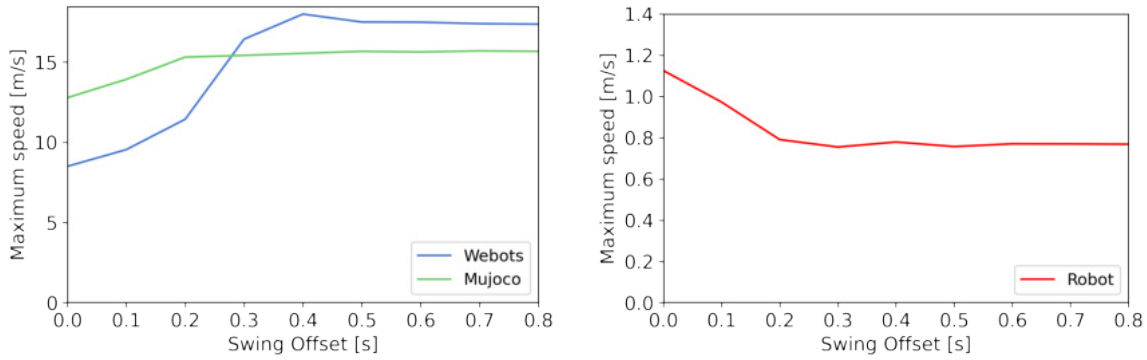

(a) Simulations **(b)** Robot

Figure 3.2: Impact of the swing offset on the speed at the point of impact

On the other hand, the body offset parameter (Figure 3.3) exhibited a similar profile than the swing offset (from -40% for Webots, -18% for Mujoco), but the decrease in speed was more significant with higher offset values and appeared in both simulations (-34% for Webots, -18% for Mujoco). A small decreases seem to appear with the robot experimentations as well, but it is not significant. Those results suggest that the synchronization of both movement is important to maximize the impact velocity.

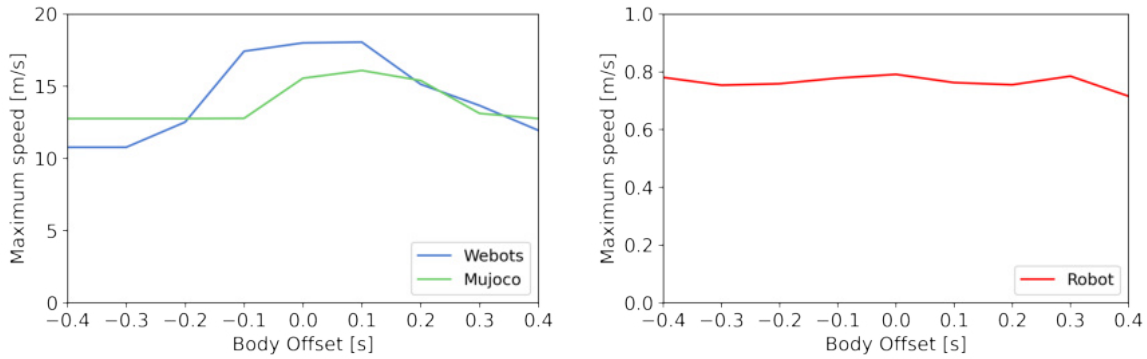

(a) Simulations **(b)** Robot

Figure 3.3: Impact of the body offset with the swing on the speed at the point of impact

Increasing the body rotation speed (Figure 3.5) and maximum body rotation (Figure 3.4) had a substantial positive impact on the maximum impact speed, both in simulations and during robotic testing. The percentage differences compared to baseline parameters without body rotation are - 35%, -23% and -25% for Webots, Mujoco and the robot respectfully. For a body rotation of 60° the percentage differences are + 16%, +28% and +6%. For a body rotation velocity of 0, the differences are -35%, -23% and -25%. For a body rotation velocity of 10 rad/s for the simulations and 300 rev/min for the robot, the differences are 31%, 34% and 26%. Indicating that synchronizing the body movement with the tail swing is important to maximize the effectiveness of the impact.

Increasing the half-angle of mobility (Figure 3.7) in the tendon-driven simulation always increases the maximum speed of impact (from -30 % to 24%), however, this is not always

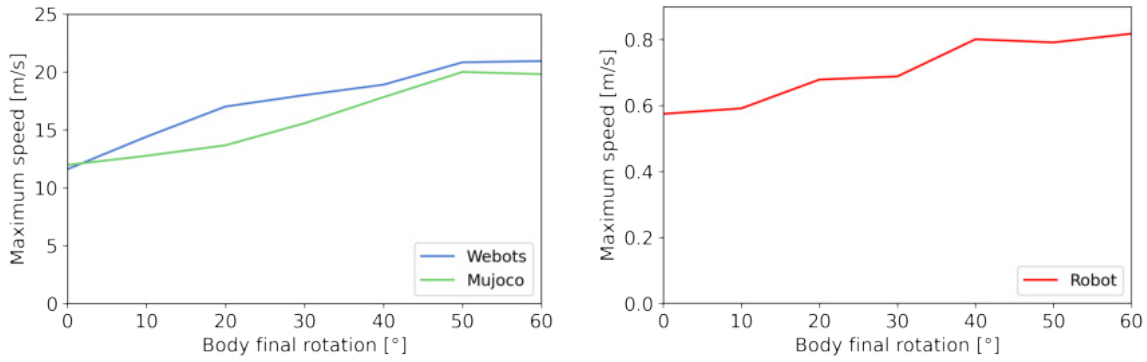

(a) Simulations **(b)** Robot

Figure 3.4: Impact of the body rotation angle on the speed at the point of impact

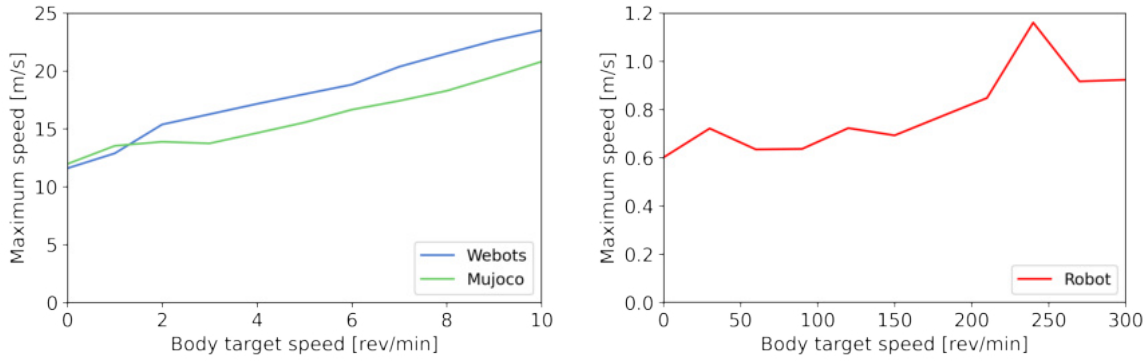

(a) Simulations **(b)** Robot

Figure 3.5: Impact of the body rotation target velocity on the speed at the point of impact

true for the motor simulation when the swing is combined with the body rotation. The speed stays relatively stable, with a maximum value obtained with an angle of 10°. This is likely due to some mismatch between the body maximum speed and the tail maximum speed when the angle of mobility gets too high. Without body rotation, the maximum velocity always increases with the half-angle of mobility.

Figure 3.8 depict the different tendon control speed tested on Mujoco over the range of swing offset value. The highest maximum speed is reached with a step of 0.03 and a swing offset of 0.2 (+4% increase compared with the maximum value obtained with a step of 1). This suggests that reducing the muscle contraction speed benefits from a higher conservation of energy coming from the preliminary blow. The motor speed to club speed relation on the robot is depicted on Figure 3.9. The graph suggests that the maximum speed of the club is a linear function of the motor maximum velocity.

If the maximum velocity of the swing was between 10 and 20 m/s. This would result in an impulse between 440 and 880 kg·m/s. Figure 3.10a provides insights into the potential force of impact based on the stopping time. Comparable shocks have stopping times ranging from 0.05 to 0.3 seconds [3]. With a stopping time of 0.1 s, the force of impact would range from 4400 to 8800 N and the kinetic energy of the club would be between 2.2 and 8.8 kJ. The stress of impact depending on the area of impact is shown on Figure 3.10b. If the club was equipped with spikes, the impact area would have approximately been $0.2\,\text{cm}^2$ [3]. With

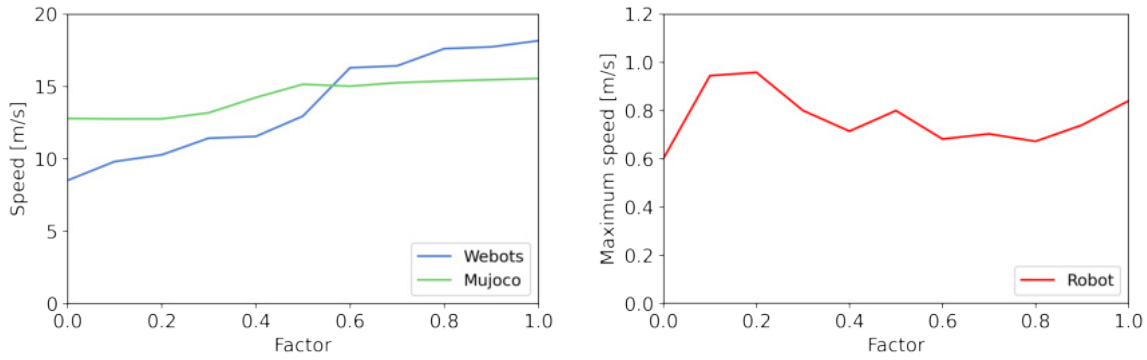

(a) Simulations **(b)** Robot

Figure 3.6: Impact of the factor of power of the preliminary blow on the speed at the point of impact

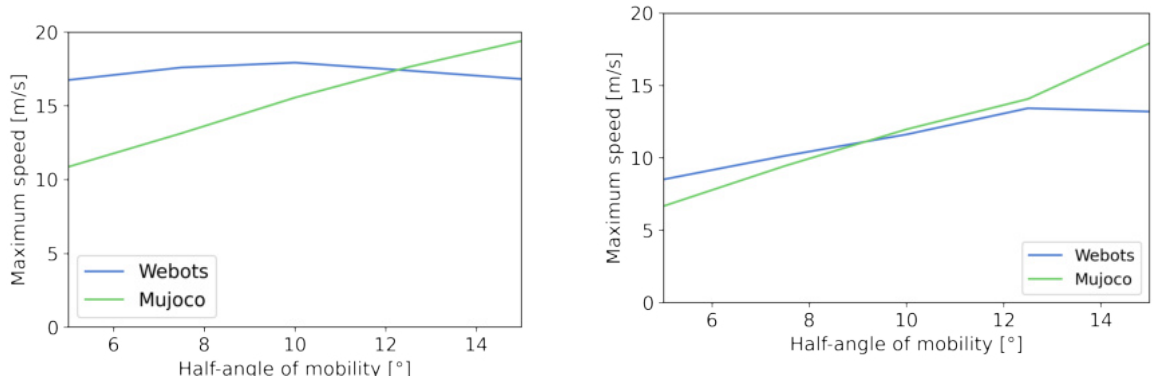

(a) With body rotation **(b)** Without body rotation

Figure 3.7: Impact of the half-angle of mobility on the speed of impact

a force of impact of, 6600 N, the impact stress would then be 330 MPa. Considering living cortical bone have a maximum shear strength of approximately 100 MPa [3][6], it is likely that the club could fracture bones.

Figures 3.11 to 3.16 depict the cost of impact in comparison with the different parameters. For the swing and body offset, the cost is inversely proportional to the velocity of the club, as expected, since those parameters are not supposed to impact the energy cost. However, both the body rotation and the body rotation maximum speed significantly reduced the energy cost of impact, as depicted in Figure 3.13 and 3.14. This is confirmed with the robot results as well.

The factor of power (Figure 3.6) and half-mobility angle (Figure 3.16) shows very different curves depending on the testing subjects. For Webots, the cost decreases with the factor and increases with the half-mobility angle. For Mujoco it stays relatively stable, but still tends to decrease with the factor of power and is heavily reduced with the half-angle of mobility. For the robot, it tends to increase with the factor of power. Reducing the factor of power did not reduce the energy consumption as much as it decreased the speed of impact. Overall, the cost of impact almost always diminish when the speed of the club increases. This is due to the energy consumption value being relatively stable throughout the experimentations, especially for the tail.

The highest speed reached in the Mujoco simulations was 20.8 m/s with a body maximum

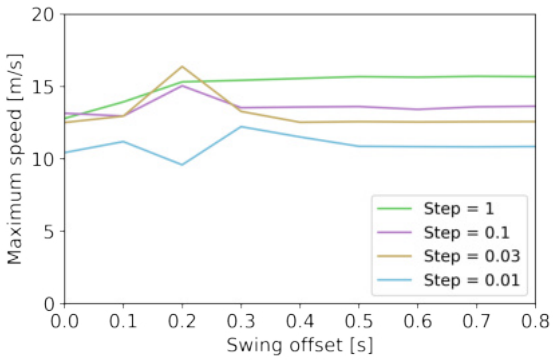

Figure 3.8: Impact of the tendon step in Mujoco

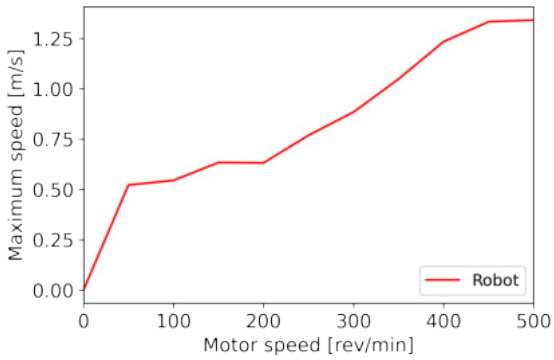

Figure 3.9: Impact of the speed of the motor on the speed of impact

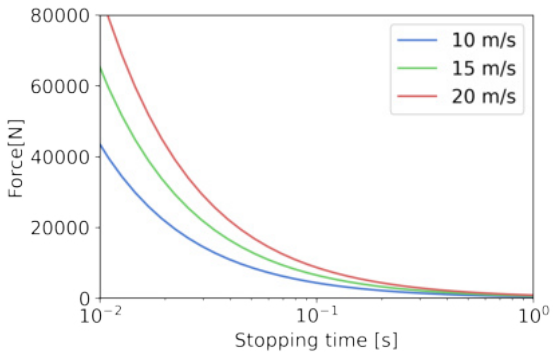

(a) Force of impact in function of the time of impact, with different speed values

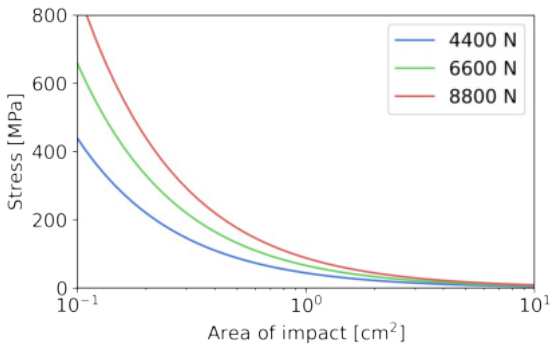

(b) Stress of impact in function of the area of impact, with different force values

Figure 3.10: Stress and force of impact

angular velocity of 10 rad/s. Without rotation, the velocity of the club was 11.96 m/s. The minimum velocity was 10.86 m/s with a 5 degree half-angle of mobility. The maximum velocity with baseline parameters was 15.54 m/s. For Webots, the baseline was 17.9 m/s, the minimum velocity reached was 8.50 m/s with a swing offset of 0 s and the maximum was 23.51 m/s with a body maximum angular velocity of 10 rad/s.

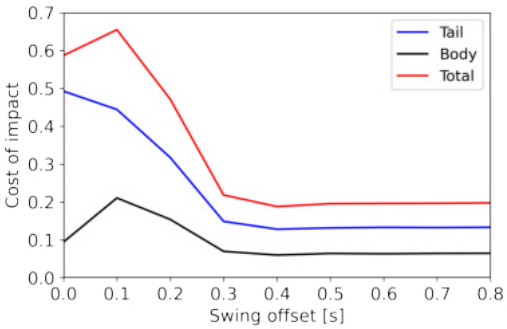

(a) Webots

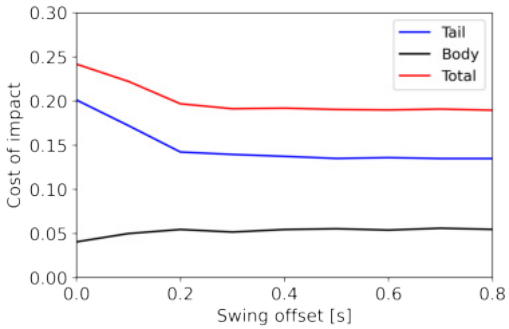

(b) Mujoco

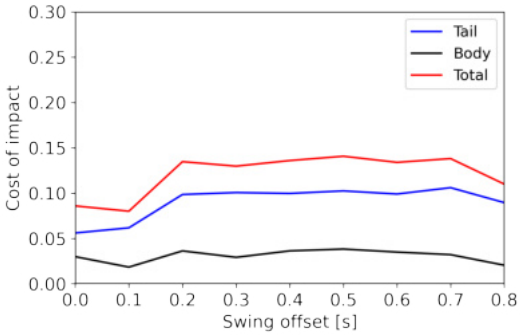

(c) Robot

Figure 3.11: Impact of swing offset on the cost of impact

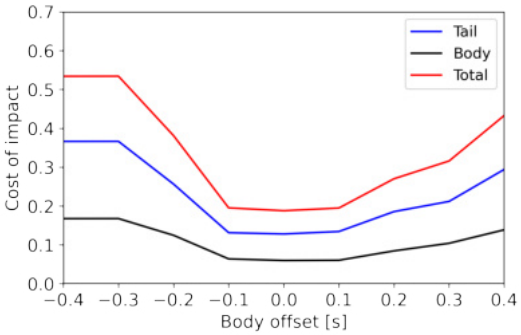

(a) Webots

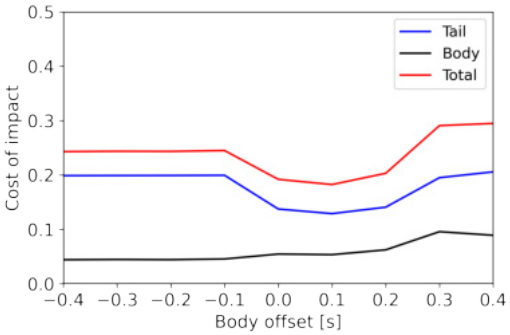

(b) Mujoco

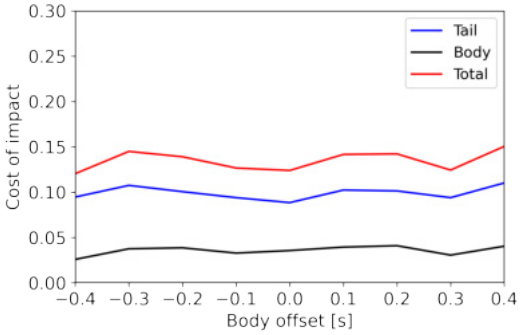

(c) Robot

Figure 3.12: Impact of body rotation offset on the cost of impact

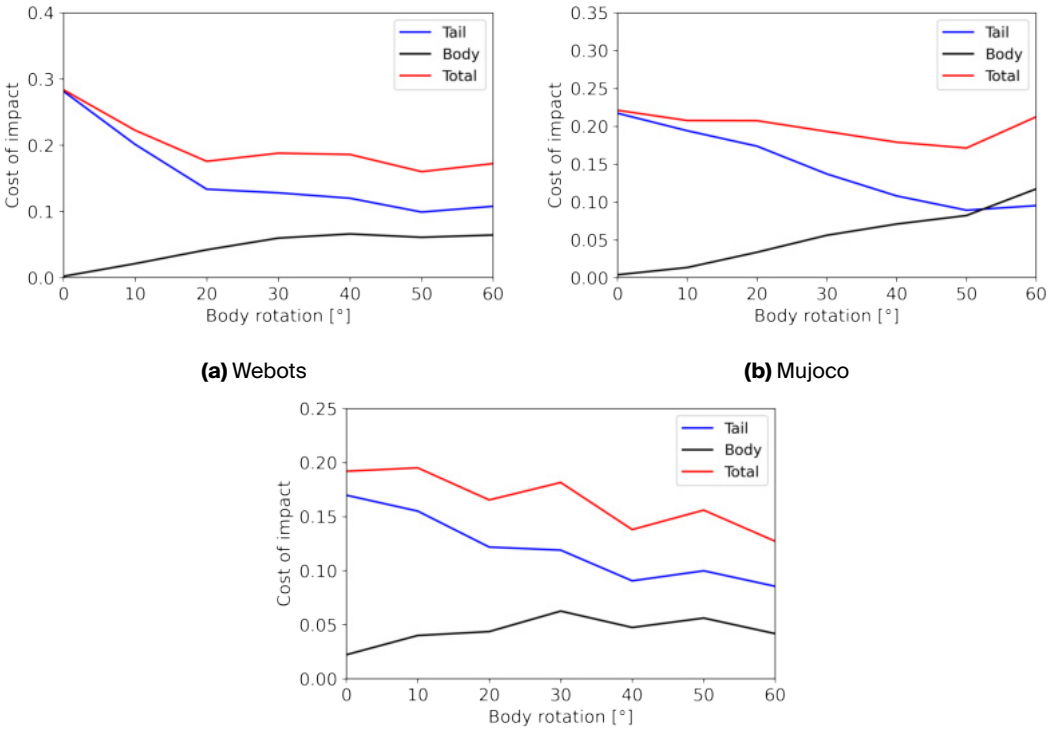

(a) Webots **(b)** Mujoco

(c) Robot

Figure 3.13: Impact of the body rotation on the cost of impact

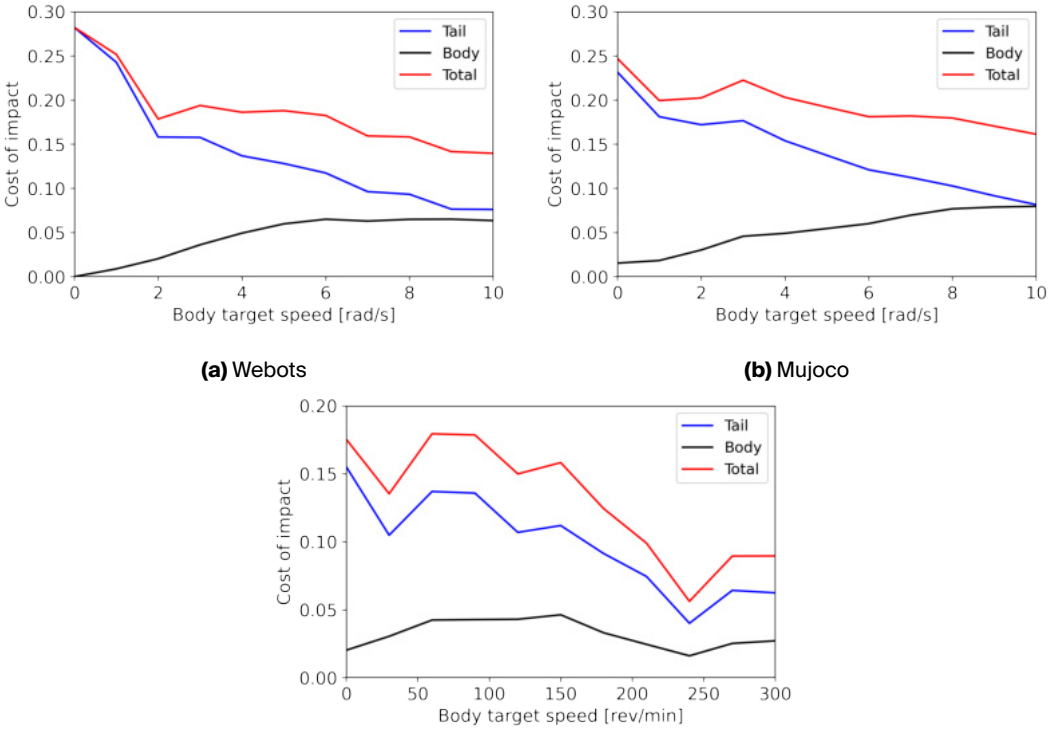

(a) Webots **(b)** Mujoco

(c) Robot

Figure 3.14: Impact of the body target velocity on the cost of impact

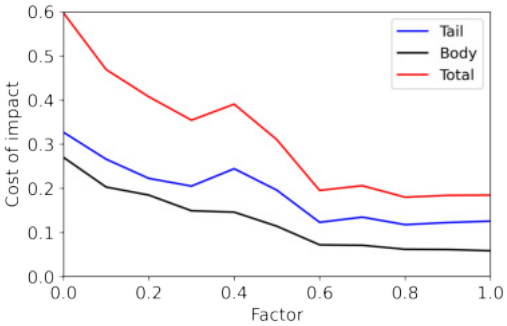

(a) Webots

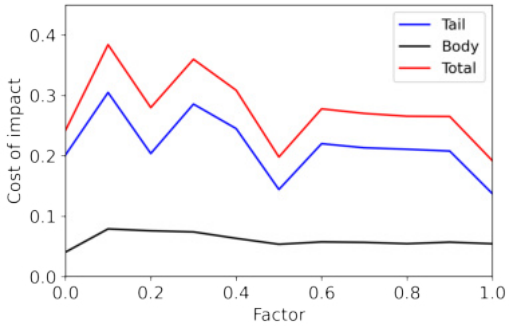

(b) Mujoco

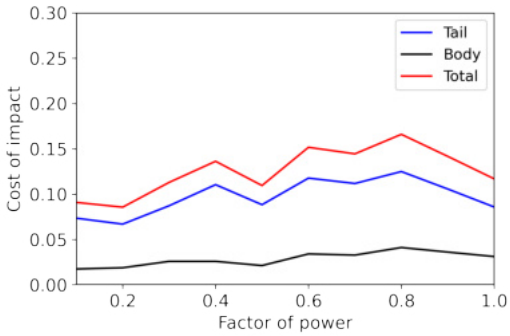

(c) Robot

Figure 3.15: Impact of the factor of power on the cost of impact

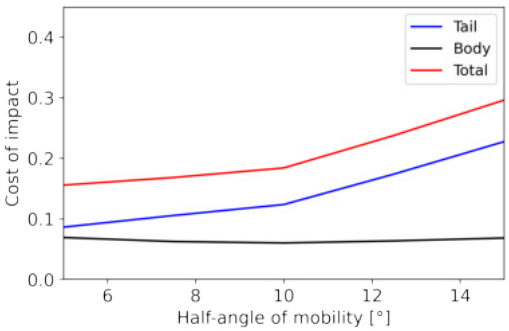

(a) Webots

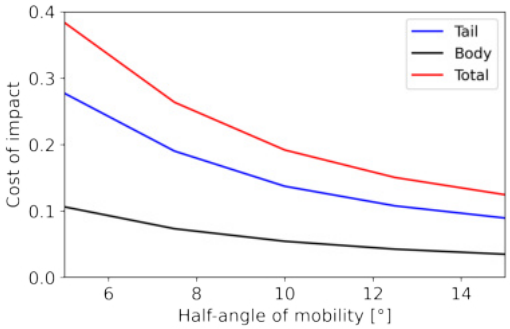

(b) Mujoco

Figure 3.16: Impact of the half-angle of mobility on the cost of impact

4. Discussion

Varying the experimentation parameters led to speed of impact ranging from 5 to 25 m/s. With an optimal motion and a reasonable range of movement, a *Doedicurus* club's tip could probably reach a velocity of 20 m/s. To achieve such velocity, a movement of the body synchronized with the tail blow was necessary, to maximize the force of impact as well as the energy efficiency. This is confirmed both by the simulations and the robots testing.

A preliminary movement of the tail in the opposite direction also had to be important to maximize damages. This is less apparent when looking at the robot results, which can be attributed to the rigidity of the tendon system and the torques available to the motors being too high, resulting in a very high acceleration compared to the size of the tail and limiting the effects of the range of movements. Such a preliminary movement may also have been directed diagonally upward, for the swing power to be increased by gravity in a downward motion. Such a movement could be tested by adapting the design of the simulations and robotic model.

The range of tail velocity is in accordance with Alexander R.M. and colleagues [2] findings. While the amount of energy provided by the rest of the body was heavily underestimated in their calculations, the amount of energy which would be transmitted to the club was also heavily overestimated. Indeed, a good portion of kinetic energy is used to move the proximal part of the tail. This confirms the likelihood of the tail being able to fracture the carapace during intra-specific combat, as the maximum kinetic energy of the club could very well go past the upper bound estimation of 6 kJ for a fracture.

A cost of impact was defined to provide insights into the energy efficiency of the strikes. This cost could be used as an objective function for optimization algorithms. Optimization techniques are often used in the field of biorobotics to find the optimal movements or behaviour linked with a specific motion [26] [25]. This could be implemented into the experimentation to find the optimal strategy of tail motion.

The prototype of the robotic tail was developed using a trial-and-error method, taking into account certain aspects of the biological tail and incorporating them into the robot's design. However, other aspects, such as the precise dynamics of the tendons and the relationship between motor actuation and tail velocity, received only limited attention prior to prototyping. The control system for the robot was also simplified in comparison to the complexity of real tail actuation. To achieve a closer resemblance to biological dynamics, future adaptations are necessary both in terms of the robot's design and its control system.

An alternative model-informed design approach can be used to design similar animal-inspired robots. Mathematical models can be useful to compute the robot shape from knowledge of the motion and to solve the transformations between the actuator space and the tail's position [24]. However, those models are expensive computationally, which is why they have been adapted into a machine-learning approach. Solving simple neural network can be an avenue for designing and controlling sophisticated robotic systems that closely mimic the motions and capabilities of their animal counterparts.

Going forward, there is potential for further refinement of robotic models and simulations to more accurately replicate the natural movements and dynamics of a real tail. Some at-

tempts have been made to incorporate this effect, but didn't result in significant impact over the experimentations. The current tendon-driven simulations and robotic systems utilize rigid tendons that lack the complexity of real tendons. Introducing some degree of elasticity to the system could aid in achieving a closer resemblance to biological muscles. However, careful consideration is necessary to prevent the model from becoming excessively elastic.

The experimentation process could use some improvement. With an adapted tendon-motor speed, it would be possible to get a movement velocity which relates more closely to the ones in the simulations. The body rotation impact would also be more visible this way. Furthermore, to limit the impact from the variations of tensions in the strings, the string tightness should be adapted between each experiment. This would greatly increase the time of experimentations, but would insure the system is as stable as possible.

The body mass of the robotic model is also too low in comparison with the tail mass, which could impact the transfer of kinetic energy. This was taken into account in the calculations but could be included directly in the robotic model, with an improved plate rotation.

Additionally, investigations into the structural properties of the tail club and of the carapace, such as its deformation under impact, could help to estimate the forces on impact and the potential fracture which could have happened during intra-specific fighting.

5. Conclusion

Through simulations and robotic experiments, this thesis investigated the biomechanics and functionality of the tail club in *Doedicurus*. The findings offer valuable insights into the determinants of impact force, energy efficiency, and damage potential associated with the tail club. The movement properties were analysed using a robotic model and two different simulations. The focus was made on the maximum velocity and energy efficiency of the tail swing, as optimizing those parameters was in the best interest of the animal. The focus was made on a lateral movement which was synchronized with a rotation of the body.

The results suggest that body movement, in combination with tail motion, play a crucial role in maximizing the force of impact and energy efficiency during strikes. The preliminary movement of the tail in the opposite direction appears to be a key factor for maximizing damage inflicted on opponents. However, the robotic experiments exhibited limitations due to the rigidity of the tendon system and the restricted range of movements, resulting in differences compared to simulation results. The observed range of tail velocities aligns with previous research, confirming the likelihood of the tail club being capable of fracturing the carapace during intra-specific combat. Such combat would have been the main selective pressure that influenced the evolution of the tail club, as individuals with more formidable and efficient tail clubs were likely favoured by sexual selection.

Such investigations contribute to our broader understanding of the adaptive strategies employed by organisms to thrive in their environments and provide clues about the selective pressures that influenced the evolution of the tail club. These findings contribute to our understanding of the biomechanics of *Doedicurus* and provide insights into the design and functionality of tail-inspired mechanism. Furthermore, the comparison between simulations and robotic experiments has shed light on some of the limitations and possibilities in the field of Biorobotics.

References

[1] R. McNeill Alexander. “Mechanics of fighting by extinct animals”. In: *Physics Education* 36.5 (2001), p. 415.

[2] R. McNeill Alexander, RICHARD A FARIÑA, and SERGIO F VIZCAÍNO. “Tail blow energy and carapace fractures in a large glyptodont (Mammalia, Xenarthra)”. In: *Zoological Journal of the Linnean Society* 126.1 (1999), pp. 41–49.

[3] Victoria M. Arbour. “Estimating impact forces of tail club strikes by ankylosaurid dinosaurs”. In: *PLoS One* 4.8 (2009), e6738.

[4] Victoria M. Arbour and Lindsay E. Zanno. “Tail weaponry in ankylosaurs and glyptodonts: an example of a rare but strongly convergent phenotype”. In: *The Anatomical Record* 303.4 (2020), pp. 988–998.

[5] R. Ernesto Blanco, Washington W Jones, and Andrés Rinderknecht. “The sweet spot of a biological hammer: the centre of percussion of glyptodont (Mammalia: Xenarthra) tail clubs”. In: *Proceedings of the Royal Society B: Biological Sciences* 276.1675 (2009), pp. 3971–3978.

[6] Kenneth Carpenter et al. “Evidence for predator-prey relationships: examples for Allosaurus and Stegosaurus”. In: *The carnivorous dinosaurs* (2005), pp. 325–350.

[7] James Dwight Dana. *Manual of geology*. 1894.

[8] Thomas Defler and Thomas Defler. “The Xenarthrans: Armadillos, Glyptodonts, Anteaters, and Sloths”. In: *History of Terrestrial Mammals in South America: How South American Mammalian Fauna Changed from the Mesozoic to Recent Times* (2019), pp. 117–138.

[9] Michael H Dickinson, Fritz-Olaf Lehmann, and Sanjay P Sane. “Wing rotation and the aerodynamic basis of insect flight”. In: *Science* 284.5422 (1999), pp. 1954–1960.

[10] Gordon Dzemski and Andreas Christian. “Flexibility along the neck of the ostrich (Struthio camelus) and consequences for the reconstruction of dinosaurs with extreme neck length”. In: *Journal of Morphology* 268.8 (2007), pp. 701–714.

[11] Andrea Elissamburu. “Bipedalism in Glyptodon Clavipes (Mammalia, Xenarthra): the results of a biomechanical model.” In: ().

[12] Richard Fariña. “Taphonomy and palaeoecology of the South American giant mammals”. In: *Current Topics In Taphonomy and Fossilization, Valencia: Ayuntamiento De Valencia* (Jan. 2002), pp. 97–113.

[13] RICHARD A FARIÑA. “Limb bone strength and habits in large glyptodonts”. In: *Lethaia* 28.3 (1995), pp. 189–196.

[14] J Ferigolo, AJG Araujo, and LF Ferreira. “Non-human vertebrate paleopathology of some Brazilian Pleistocene mammals”. In: *Paleopatologia and Paleoepidemiologia-Estudos Multidisciplinares (Araujo, A. & Ferreira, L., Eds.), Panorama/Escola Nacional de Saude Publica, Rio de Janeiro* (1992), pp. 213–234.

[15] Qiang Huang et al. “Planning walking patterns for a biped robot”. In: *IEEE Transactions on robotics and automation* 17.3 (2001), pp. 280–289.

[16] Auke Ijspeert. “Biorobotics: Using robots to emulate and investigate agile locomotion”. In: *science* 346.6206 (2014), pp. 196–203.

[17] Auke Ijspeert et al. “From swimming to walking with a salamander robot driven by a spinal cord model”. In: *science* 315.5817 (2007), pp. 1416–1420.

[18] Yusuke Ikeda et al. “Analysis of trunk muscle activity in the side medicine-ball throw”. In: *The Journal of Strength & Conditioning Research* 23.8 (2009), pp. 2231–2240.

[19] Sangbae Kim et al. “Smooth vertical surface climbing with directional adhesion”. In: *IEEE Transactions on robotics* 24.1 (2008), pp. 65–74.

[20] Anne D Koelewijn, Dieter Heinrich, and Antonie J van den Bogert. “Metabolic cost calculations of gait using musculoskeletal energy models, a comparison study”. In: *PloS one* 14.9 (2019), e0222037.

[21] George V Lauder et al. “Fish biorobotics: kinematics and hydrodynamics of self-propulsion”. In: *Journal of experimental biology* 210.16 (2007), pp. 2767–2780.

[22] Kévin Le Verger. “Xenarthrans of the collection of Santiago Roth from the Pampean Region of Argentina (Pleistocene), in Zurich, Switzerland”. In: *Swiss Journal of Palaeontology* 142.1 (2023), pp. 1–39.

[23] Ryan D Maladen et al. “Undulatory swimming in sand: subsurface locomotion of the sandfish lizard”. In: *science* 325.5938 (2009), pp. 314–318.

[24] Gianmarco Mengaldo et al. “A concise guide to modelling the physics of embodied intelligence in soft robotics”. In: *Nature Reviews Physics* 4.9 (2022), pp. 595–610.

[25] John A Nyakatura et al. “Reverse-engineering the locomotion of a stem amniote”. In: *Nature* 565.7739 (2019), pp. 351–355.

[26] Robert Siddall et al. “Mechanisms for Mid-Air Reorientation Using Tail Rotation in Gliding Geckos”. In: *Integrative and Comparative Biology* 61.2 (June 2021), pp. 478–490. ISSN: 1540-7063.

[27] Alexander Spröwitz et al. “Towards dynamic trot gait locomotion: Design, control, and experiments with Cheetah-cub, a compliant quadruped robot”. In: *The International Journal of Robotics Research* 32.8 (2013), pp. 932–950.

[28] “Strain and elongation of the human gastrocnemius tendon and aponeurosis during maximal plantarflexion effort”. In: *Journal of Biomechanics* 38.4 (2005), pp. 833–841. ISSN: 0021-9290.

[29] Sergio F Vizcaino et al. “Proportions and function of the limbs of glyptodonts”. In: *Lethaia* 44.1 (2011), pp. 93–101.

[30] Martin Zamorano, Alvaro Mones, and Gustavo Juan Scillato Yané. “Redescripción y designación de un neotipo de Panochthus tuberculatus (Owen)(Mammalia, Cingulata, Glyptodontidae)”. In: *Revista Brasileira de Paleontologia* 15 (2012).